Analog Sauter-Schwinger effect in semiconductors for spacetime-dependent fields

Malte F. Linder, Axel Lorke, and Ralf Schützhold[*]

Fakultät für Physik, Universität Duisburg-Essen, Lotharstr. 1, 47057 Duisburg, Germany

The Sauter-Schwinger effect predicts the creation of electron-positron pairs out of the quantum vacuum via tunneling induced by a strong electric field. Unfortunately, as the required field strength is extremely large, this fundamental prediction of quantum field theory has not been verified experimentally yet. Here, we study under which conditions and approximations the interband tunneling in suitable semiconductors could be effectively governed by the same (Dirac) Hamiltonian, especially for electric fields which depend on space and time. This quantitative analogy would allow us to test some of the predictions (such as the dynamically assisted Sauter-Schwinger effect) in this area by means of these laboratory analogs.

I. INTRODUCTION

The are several fundamental predictions of quantum field theory which have so far resisted a direct experimental verification. One of the most prominent examples is the Sauter-Schwinger effect [1–4] predicting the creation of electron-positron pairs out of the quantum vacuum via tunneling. For a constant electric field E, the associated pair-creation probability behaves as

$$P_{e^+e^-} \propto e^{-\pi E_{\mathrm{crit}}^{\mathrm{QED}}/E} \tag{1}$$

and is thus exponentially suppressed for fields E well below the critical field

$$E_{\mathrm{crit}}^{\mathrm{QED}} = \frac{m^2 c^3}{\hbar q} \approx 1.3 \times 10^{18}\, \frac{\mathrm{V}}{\mathrm{m}} \tag{2}$$

(often denoted by E_S in the literature), where m is the electron mass and $q > 0$ the elementary charge. The fact that expression (1) does not admit a Taylor expansion in q already indicates that this is a nonperturbative effect, which renders calculations intrinsically difficult. Nevertheless, apart from the constant-field case above, it is possible to derive the pair-creation probability for several scenarios with varying fields. For example, a temporal Sauter pulse of the form $E(t) = E_0/\cosh^2(\omega t)$ does also facilitate an exact solution of the Dirac equation (see, e.g., Ref. [5]). In this situation, the absolute value of the exponent (1) is reduced and thus the probability enhanced. Conversely, for a spatial Sauter profile $E(x) = E_0/\cosh^2(kx)$, the absolute value of the exponent increases, leading to a suppression of the pair-creation probability.

As another interesting case, the superposition of a constant (or slowly varying) strong field with a weaker time-dependent field can result in an enhancement of the probability: the dynamically assisted Sauter-Schwinger effect [6]. The dependence of this effect on the shape of the weaker time-dependent field and the momentum of the created electrons and positrons has been studied in Refs. [7–10], for example. If the strong field is not constant but spatially varying (such as a spatial Sauter profile), there is an interesting interplay or competition between the spatial dependence of the stronger field and the temporal dependence of the weaker field; see Ref. [11].

Most unfortunately, because the critical field strength (2) is so large, these nonperturbative phenomena have not been observed yet, and thus it was not possible to test the various predictions mentioned above experimentally. This motivates the quest for other, experimentally more accessible, laboratory systems which display analogous effects, ideally governed by the same Hamiltonian (under appropriate approximations) and thus the same equations of motion. To use the famous quote by R. Feynman: "*The same equations have the same solutions.*" Due to their high degree of experimental control, one such option are ultracold atoms in optical lattices; see also Refs. [12–14]. Other possible options include graphene [15–17] and trapped ions [18]. In the following, we study interband tunneling in semiconductors as another promising example. Note that the qualitative analogy between Landau-Zener tunneling in semiconductors [19–21] and the Sauter-Schwinger effect in the case of a constant electric field has already been discussed in, e.g., Refs. [16,22–26]. Here, the goal is to derive a quantitative analogy (in the spirit of Feynman) and to specify the underlying approximations and assumptions, with special emphasis on fields depending on time (see also Ref. [26]) and space (as motivated above). The use of these analogies is twofold: On the one hand, they allow us to test the above predictions by means of laboratory analogs, which are easier to access experimentally, and, on the other hand, they help us to understand the physics of these laboratory systems better.

II. TIME-DEPENDENT CASE $E = E(t)$

Let us start with the simpler case of a homogeneous and purely time-dependent external electric field in 1+1 space-time dimensions. We choose to describe the external electric field in temporal gauge $E(t) = \dot{A}(t)$ with the one-component vector potential $A(t)$. This potential couples to the electron momentum operator via the covariant derivative $\partial_x + iqA(t)$ ($c = \varepsilon_0 = \hbar = 1$ in the following, unless otherwise stated).

_____

[*]ralf.schuetzhold@uni-due.de

The many-body Dirac Hamiltonian can be written as

$$\hat{H}_D(t) = \int_{-\infty}^{\infty} \underline{\hat{\Psi}}^{\dagger} \{[-i\partial_x + qA(t)]\sigma_x + m\sigma_z\} \underline{\hat{\Psi}} \, dx. \quad (3)$$

This form is obtained by expressing the Dirac matrices in terms of Pauli matrices via $\gamma^0 = \sigma_z$ and $\gamma^1 = i\sigma_y$. The field operator consequently has two components, $\underline{\hat{\Psi}}(t,x) = (\hat{\Psi}_+(t,x), \hat{\Psi}_-(t,x))$, which corresponds to the absence of spin in 1+1 dimensions.

We transform this Hamiltonian to momentum space by inserting the spatial Fourier transform

$$\underline{\hat{\Psi}}(t,x) = \frac{1}{\sqrt{2\pi}} \int_{-\infty}^{\infty} \underline{\tilde{\hat{\Psi}}}(t,k) e^{ikx} \, dk \quad (4)$$

of the field operator. The result reads as

$$\hat{H}_D(t) = \int_{-\infty}^{\infty} \underline{\tilde{\hat{\Psi}}}^{\dagger}(t,k) \begin{pmatrix} m & k+qA(t) \\ k+qA(t) & -m \end{pmatrix} \underline{\tilde{\hat{\Psi}}}(t,k) \, dk. \quad (5)$$

The next step is to derive the crystal-momentum representation of the Hamiltonian for electrons in a semiconductor which is exposed to the same external electric field. This semiconductor Hamiltonian can then be compared to the Dirac Hamiltonian (5).

A. Two-band semiconductor model

A direct, quantitative analogy between Dirac's theory and electrons in a semiconductor can only exist if the considered semiconductor electrons can only occupy two adjacent energy bands: the higher (lower) band then corresponds to the positive (negative) relativistic continuum. In the ground state (no external field and zero temperature), the lower band must be completely filled with electrons (analog of the Dirac sea), while the upper band must be empty. This is precisely the case if we restrict the semiconductor model to the valence band and the conduction band only. Our starting point is the well-known Kane model [27], but we only include the light-hole valence band in our theory and neglect the heavy-hole band (since lighter particles are more likely to be excited via the pair-creation mechanism we are interested in) and the split-off valence band, which is energetically lowered due to spin-orbit interaction; see, e.g., Refs. [28–31], which also employ and describe this model.

Let us start with the basic Hamiltonian. Since the possible electron group velocities within the valence and conduction bands of typical semiconductors are far below the vacuum speed of light, we may describe the semiconductor electrons with the nonrelativistic Schrödinger equation. The Bloch electrons, which we are interested in, are subject to the lattice-periodic potential $V(x)$ of the ion cores. We denote the lattice constant by ℓ, so the potential satisfies $V(x + \ell) = V(x)$. For simplicity, we neglect electron-electron interactions; see Sec. VI below. The Hamiltonian of the Bloch electrons in the external field $E(t) = \dot{A}(t)$ thus reads as

$$\hat{H}_s^{\text{full}}(t) = \int_{-\infty}^{\infty} \hat{\psi}^{\dagger} \left\{ \frac{[-i\partial_x + qA(t)]^2}{2m} + V(x) \right\} \hat{\psi} \, dx, \quad (6)$$

where $\hat{\psi}(t,x)$ is the scalar electron field operator.

Note that the quadratic A term in this Hamiltonian can be absorbed via a suitable gauge transformation (see Appendix A), so we may consider the simplified Hamiltonian

$$\hat{H}_s^{\text{full}}(t) = \int_{-\infty}^{\infty} \hat{\psi}^{\dagger} \left[-\frac{\partial_x^2}{2m} + V(x) + \frac{qA(t)}{m}(-i\partial_x) \right] \hat{\psi} \, dx \quad (7)$$

instead.

For the derivation of the two-band model, we restrict the Hamiltonian $\hat{H}_s^{\text{full}}$ to valence- and conduction-band electrons only. This should be a good approximation for analogs of the Sauter-Schwinger effect since an excitation of a valence-band electron into the conduction band is associated with a lower energy difference than any other possible transition in the (initial) ground state. Larger energy differences lead to exponential suppression in the context of nonperturbative pair creation, so the two-band model should reproduce the leading-order pair-creation probability in the initial ground state correctly.

We apply the two-band approximation by assuming that only the valence and conduction Bloch bands contribute to the field operator:

$$\hat{\psi}(t,x) \approx \int_{-\pi/\ell}^{\pi/\ell} \hat{a}_-(t,K) f_-(K,x) + \hat{a}_+(t,K) f_+(K,x) \, dK. \quad (8)$$

In this equation, the functions $f_n(K,x) = \langle x|n,K\rangle$ are the position-space representations of the Bloch states $|n,K\rangle$ in the unperturbed semiconductor crystal $[A(t) = 0]$. The band index $-$ $(+)$ denotes the valence (conduction) band. There is one independent Bloch state per band for each quasimomentum K in the first Brillouin zone, which is the range $(-\pi/\ell, \pi/\ell)$. Hence, our field operator (8) is per assumption a linear combination of all Bloch states in the valence and the conduction bands at each instant of time. The time-dependent "coefficients," which are in fact operators $\hat{a}_\pm(t,K)$, are instantaneous annihilation operators for electrons in the corresponding Bloch states $|\pm,K\rangle$. For this statement to hold, the Bloch states must be normalized, so that they obey the orthonormality relation

$$\langle n,K|n',K'\rangle = \int_{-\infty}^{\infty} f_n^*(K,x) f_{n'}(K',x) \, dx$$
$$= \delta_{nn'} \delta(K' - K). \quad (9)$$

We use the convention

$$f_n(K,x) = e^{iKx} u_n(K,x) \quad (10)$$

throughout this paper, so our lattice-periodic Bloch factors $u_n(K,x)$ are orthonormalized (at a fixed K) according to the unit-cell Bloch-factor scalar product

$$\langle n,K|n',K\rangle_u = \frac{2\pi}{\ell} \int_0^{\ell} u_n^*(K,x) u_{n'}(K,x) \, dx = \delta_{nn'}. \quad (11)$$

Inserting the approximation (8) into the full Hamiltonian (7) yields the two-band semiconductor Hamiltonian $\hat{H}_s$, which neglects the dynamics of all other Bloch bands. In the calculation of $\hat{H}_s$, we use the fact that Bloch waves satisfy the energy

eigenvalue equation

$$\left[-\frac{\partial_x^2}{2m} + V(x)\right] f_n(K,x) = \mathcal{E}_n(K) f_n(K,x). \qquad (12)$$

Furthermore, the Bloch-wave momentum matrix elements $\langle n, K| - i\partial_x | n', K'\rangle$ (also known as optical matrix elements) appear in the new Hamiltonian. It is well known that these matrix elements vanish unless $K = K'$ (see, e.g., Ref. [32]; a proof of this important theorem is given in Appendix B). There are thus three independent momentum matrix elements in the two-band model for each K: the interband element κ is given implicitly by $\langle -, K| - i\partial_x | +, K'\rangle = \kappa(K)\delta(K' - K)$ [cf. Eq. (B5)] and can be written

$$\kappa(K) = \langle -, K| - i\partial_x | +, K\rangle_u \qquad (13)$$

with the product defined in Eq. (11). This quantity is complex in general; however, we define the global phases of the Bloch bands in a way such that the value $\kappa_0 = \kappa(0)$ is real and positive: $\kappa_0 > 0$. The two intraband elements are related to the group velocities $v_\pm(K) = d\mathcal{E}_\pm(K)/dK$ via

$$\langle \pm, K| - i\partial_x | \pm, K'\rangle = m v_\pm(K)\delta(K' - K); \qquad (14)$$

see, e.g., Refs. [31,33].

The resulting two-band Hamiltonian in crystal-momentum space reads as

$$\hat{H}_s(t)$$
$$= \int_{-\pi/\ell}^{\pi/\ell} \underline{\hat{a}}^\dagger(t,K)\begin{pmatrix} \mathcal{E}_+ + qAv_+ & \frac{qA}{m}\kappa^* \\ \frac{qA}{m}\kappa & \mathcal{E}_- + qAv_- \end{pmatrix}\underline{\hat{a}}(t,K)\,dK$$
$$(15)$$

(we have omitted to write explicitly the dependencies of the quantities in the matrix here) with

$$\underline{\hat{a}}(t,K) = \begin{pmatrix} \hat{a}_+(t,K) \\ \hat{a}_-(t,K) \end{pmatrix}. \qquad (16)$$

Note that this Hamiltonian as well as the Dirac Hamiltonian (5) have the form $\hat{H}(t) = \int \hat{\mathcal{H}}(t,k)\,dk$, which means that each k mode evolves independently, and k (or K in the semiconductor case) is thus a conserved quantity as expected in a purely time-dependent potential.

B. Diagonalization of the Hamiltonians

In order to bring both Hamiltonians $\hat{H}_D$ and $\hat{H}_s$ into the same form, so that we can compare them, we diagonalize the 2×2 matrices in the Hamiltonians. To this end, we transform ("rotate") the momentum-space field operators $\tilde{\hat{\Psi}}(t,k)$ (Dirac case) and the Bloch-electron operators $\underline{\hat{a}}(t,K)$ (semiconductor) to operators corresponding to the instantaneous energy eigenstates, respectively.

In the Dirac case, the transformed field operators read as

$$\underline{\hat{\Upsilon}}(t,k) = \frac{1}{\sqrt{1 + d^2(t,k)}}\begin{pmatrix} 1 & d(t,k) \\ -d(t,k) & 1 \end{pmatrix}\tilde{\hat{\Psi}}(t,k) \quad (17)$$

with the abbreviations

$$d(t,k) = \frac{k + qA(t)}{m + \Omega(t,k)} \qquad (18)$$

and

$$\Omega(t,k) = \sqrt{m^2 + [k + qA(t)]^2}. \qquad (19)$$

Note that Eq. (17) describes a unitary relation, which is also a Bogoliubov transformation, so the two components of $\underline{\hat{\Upsilon}}$ obey the canonical anticommutation relations. In terms of these field operators, the Dirac Hamiltonian (5) assumes the diagonal form

$$\hat{H}_D(t) = \int_{-\infty}^{\infty} \underline{\hat{\Upsilon}}^\dagger(t,k)\begin{pmatrix} \Omega(t,k) & 0 \\ 0 & -\Omega(t,k) \end{pmatrix}\underline{\hat{\Upsilon}}(t,k)\,dk. \quad (20)$$

Before we diagonalize the matrix in the semiconductor Hamiltonian (15), we want to make its diagonal elements symmetric like in the Dirac case, in which the original diagonal elements in Eq. (5) are $\pm m$. In order to do this, we rewrite the Hamiltonian as

$$\hat{H}_s(t)$$
$$= \int_{-\pi/\ell}^{\pi/\ell} \underline{\hat{a}}^\dagger(t,K)\begin{pmatrix} \frac{\Delta\mathcal{E} + qA\Delta v}{2} & \frac{qA}{m}\kappa^* \\ \frac{qA}{m}\kappa & -\frac{\Delta\mathcal{E} + qA\Delta v}{2} \end{pmatrix}\underline{\hat{a}}(t,K)\,dK$$
$$+ \int_{-\pi/\ell}^{\pi/\ell} \frac{\mathcal{E}_+(K) + \mathcal{E}_-(K) + qA(t)[v_+(K) + v_-(K)]}{2}$$
$$\times \underbrace{[\hat{a}_+^\dagger(t,K)\hat{a}_+(t,K) + \hat{a}_-^\dagger(t,K)\hat{a}_-(t,K)]}_{=1 \text{ for all } t \text{ and } K}\,dK. \qquad (21)$$

In this equation, we have introduced the (K-dependent) band-energy difference $\Delta\mathcal{E}(K) = \mathcal{E}_+(K) - \mathcal{E}_-(K)$ and the group-velocity difference $\Delta v(K) = v_+(K) - v_-(K)$. Since K is a conserved quantity, $\underline{\hat{a}}^\dagger(t,K)\underline{\hat{a}}(t,K)$ must always be 1 because there is exactly one electron per K value in our two-band model, and the electron for a given K must be either in the conduction band or in the valence band at each point in time. The second K integral in the Hamiltonian (21) therefore yields a time-dependent constant, which can be eliminated by a gauge transformation on the scalar potential again, as described in Appendix A.

The Bogoliubov transformation which diagonalizes the redefined semiconductor Hamiltonian [first K integral in Eq. (21)] has the same form as in the Dirac case [complex version of Eq. (17)],

$$\underline{\hat{b}}(t,K) = \frac{1}{\sqrt{1 + |\mathfrak{d}(t,K)|^2}}\begin{pmatrix} 1 & \mathfrak{d}^*(t,K) \\ -\mathfrak{d}(t,K) & 1 \end{pmatrix}\underline{\hat{a}}(t,K),$$
$$(22)$$

but with different auxiliary functions

$$\mathfrak{d}(t,K) = \frac{qA(t)\kappa(K)/m}{[\Delta\mathcal{E}(K) + qA(t)\Delta v(K)]/2 + \Omega(t,K)} \qquad (23)$$

and

$$\Omega(t,K)$$
$$= \sqrt{\left[\frac{\Delta\mathcal{E}(K) + qA(t)\Delta v(K)}{2}\right]^2 + \left[\frac{qA(t)|\kappa(K)|}{m}\right]^2},$$
$$(24)$$

(a) Relativistic dispersion relation.
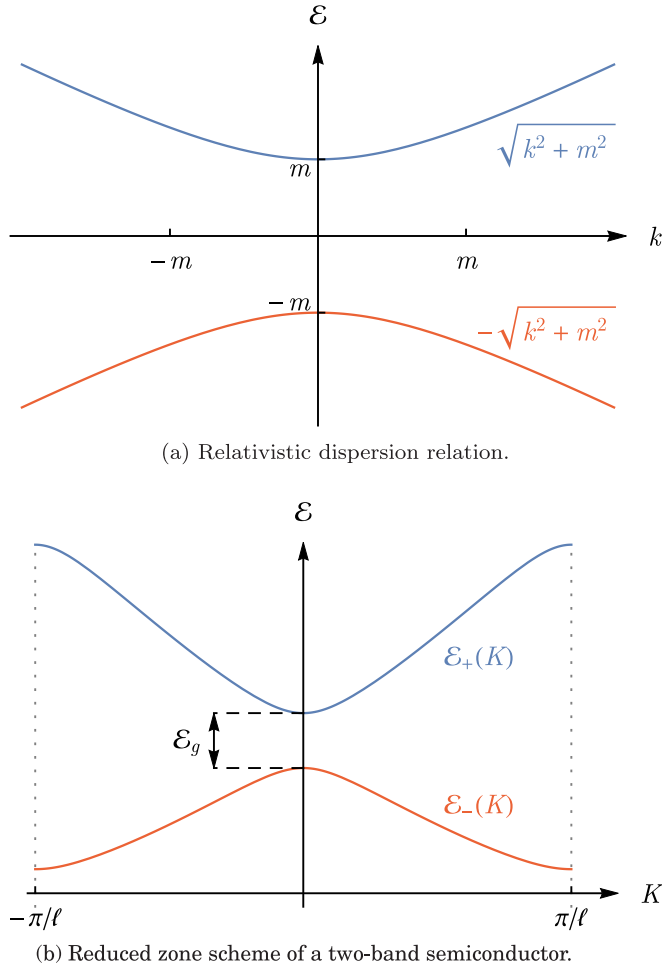

(b) Reduced zone scheme of a two-band semiconductor.

FIG. 1. Electron dispersion relations in the two systems under consideration, without an external electric field ($A = 0$). (a) Dirac case: the two branches of the relativistic energy-momentum relation. (b) Semiconductor case: example for an electronic two-band structure in the first Brillouin zone (reduced zone scheme). We assume throughout this paper that the semiconductor has a direct band gap at the center of the Brillouin zone, measuring $\mathcal{E}_g = \Delta\mathcal{E}(0)$.

so the resulting Hamiltonian reads as

$$\hat{H}_s(t) = \int_{-\pi/\ell}^{\pi/\ell} \hat{\underline{b}}^\dagger(t,K) \begin{pmatrix} \Omega(t,K) & 0 \\ 0 & -\Omega(t,K) \end{pmatrix} \hat{\underline{b}}(t,K)\, dK.$$
(25)

Now that we have derived the diagonal forms of both Hamiltonians, their physical differences including scales and dependence on conserved (quasi)momentum are encoded in the instantaneous energy eigenvalues Ω and Ω.

C. Analogy between the modes $k = 0$ and $K = 0$

Let us start to point out the quantitative analogy between the two Hamiltonians $\hat{H}_D$ (20) and $\hat{H}_s$ (25), at the (quasi)momentum-space points $k = K = 0$. We assume for the moment that there is no electric field ($A = 0$).

The energy bands in the Dirac case are the two square roots of the relativistic energy-momentum relation; see Fig. 1(a).

The mode $k = 0$ thus coincides with the minimal mass gap $2m$ in the absence of an external field.

The exact shapes of the valence band and the conduction band in the semiconductor $\mathcal{E}_\pm(K)$ are not fixed but depend on the periodic potential $V(x)$; however, we make the following assumptions about the semiconductor band structure, which shall be satisfied in the remainder of this paper:

(i) no band crossing [$\Delta\mathcal{E}(K) > 0$ for each K] and

(ii) a direct band gap at the center $K = 0$ of the Brillouin zone; that is, $\mathcal{E}_g = \Delta\mathcal{E}(0)$ is the minimal value of $\Delta\mathcal{E}(K)$.

An example for such a band structure is plotted in Fig. 1(b).

Now, we reintroduce the electric field and compare the instantaneous energy eigenvalues in Eqs. (19) and (24) at $k = K = 0$ with each other. In the Dirac case, we get

$$\Omega(t,0) = \sqrt{(mc^2)^2 + [cq\,A(t)]^2}$$
(26)

with the speed of light written explicitly in this equation. In the semiconductor case, we first note that both group velocities [$\mathcal{E}_\pm(K)$ derivatives] vanish at $K = 0$ and thus also $\Delta v(0) = 0$. Comparing the resulting $\Omega(t,0) = \sqrt{(\mathcal{E}_g/2)^2 + [q\,A(t)\kappa_0/m]^2}$ with Eq. (26), we immediately see that the quantity $c_\star = \kappa_0/m$ plays the role of an effective speed of light in the semiconductor.

We also want to define a suitable effective mass $m_\star$ such that $m_\star c_\star^2$ (the analog of the rest energy mc^2 in Dirac theory) produces the term $\mathcal{E}_g/2$ in $\Omega(t,0)$ above. Hence, we set

$$m_\star = \frac{m^2 \mathcal{E}_g}{2\kappa_0^2},$$
(27)

so we may write

$$c_\star = \sqrt{\frac{\mathcal{E}_g}{2m_\star}}$$
(28)

and

$$\Omega(t,0) = \sqrt{(m_\star c_\star^2)^2 + [c_\star q\,A(t)]^2}.$$
(29)

Comparing Eqs. (26) and (29) shows that the Hamiltonians of both systems are equivalent in the large-wavelength limit $k = K = 0$. The semiconductor just exhibits different scales, which are given by the material constants $\mathcal{E}_g$ and κ_0. The same effective constants have also been found in Refs. [28,29].

Note that we refer to the quantity (27) as "effective mass" because it allows us to write $\Omega(t,0)$ in a way formally equivalent to $\Omega(t,0)$ above. Nevertheless, as we will see in the next subsection, $m_\star$ is indeed related to the parabolic energy-band curvatures in the semiconductor, which is the usual notion of effective masses in this area of physics.

Another point to notice here is that we could also define an effective elementary charge via $cq_\star = q\kappa_0/m$ instead of the effective speed of light (28) to make the analogy between the modes $k = K = 0$ work (in which case the effective electron mass in the semiconductor must be defined by the equation $m_\star c^2 = \mathcal{E}_g/2$). Or, we can shift the factor in $q_\star$ into an effective vector potential defined by $q_\star A(t) = q\,A_\star(t)$. The concept of an effective external potential in analogs of the Sauter-Schwinger effect is known from ultracold atoms in optical lattices; see Refs. [12,13]. However, we will see in the next subsection that defining an effective speed of light as above (and thus leaving

the external potential and elementary charge unchanged) is required to extend the analogy in the semiconductor to more modes than just $k = K = 0$.

D. Analogy for long-wavelength modes

We now want to extend the analogy to all small (quasi)momenta, which means $|k| \ll m$ in the Dirac case and $|K| \ll \pi/\ell$ in the semiconductor case. In this range, the dispersion curves in Fig. 1 are approximately parabolic in both cases. This is also the range with the smallest energy difference between the bands, and we consequently expect the corresponding modes to generate the dominant contributions to the total pair-creation yield via the Sauter-Schwinger effect. Note that if the vector potential vanishes in the *in* and *out* states [i.e., $A(t \to \pm\infty) = 0$], then the conserved quantities k and K correspond to the initial *and* the final kinetic (quasi)momentum of the considered mode, respectively, so the long-wavelength modes can be identified with electron states close to the minimal band gaps in Fig. 1 in this case. Given a particular external field $E(t)$, we can always satisfy this condition by letting $A(t)$ start at zero for $t \to -\infty$, and, if $A(t) \neq 0$ after the field has been switched off (or has become very tiny), letting $A(t)$ approach zero again very slowly (adiabatically, such that this process does not cause band transitions).

Concerning the analogy, let us start with the Dirac case again. The Taylor expansion of Ω around $k = 0$ reads as

$$\Omega(t,k) = \Omega(t,0) + \frac{c^2 q A(t)}{\Omega(t,0)} k + \mathcal{O}(k^2) \qquad (30)$$

with c written explicitly. In the second-order term, the small quantity $(k/m)^2$ is suppressed by the prefactor $1/\{2[1 + q^2 A^2(t)/m^2]^{3/2}\} \leqslant 1/2$. Hence, we will only consider the first orders of k or K in Ω and Ω when comparing the Hamiltonians for small (quasi)momenta, and we ignore all higher-order terms.

In the semiconductor case, we get

$$\Omega(t,K) = \Omega(t,0) + \frac{K}{\Omega(t,0)}$$
$$\times \left\{ \frac{\Delta\mathcal{E}^{(1)}(0) + q A(t)\Delta v^{(1)}(0)}{4}\mathcal{E}_g \right.$$
$$\left. + \left[\frac{q A(t)}{m}\right]^2 \kappa_0 \operatorname{Re}\kappa^{(1)}(0) \right\} + \mathcal{O}(K^2). \qquad (31)$$

Superscripts of the form "(n)" denote the nth derivative with respect to K.

In order to evaluate these derivatives at $K = 0$, we first note that the parabolic parts of the energy bands around the minimal gap are usually written as (we arbitrarily locate the band gap symmetrically around the zero energy level)

$$\mathcal{E}_+(K) = \frac{\mathcal{E}_g}{2} + \frac{K^2}{2m_{\star,e}} + \mathcal{O}(K^3),$$
$$\mathcal{E}_-(K) = -\frac{\mathcal{E}_g}{2} - \frac{K^2}{2m_{\star,h}} + \mathcal{O}(K^3), \qquad (32)$$

where $m_{\star,e}$ and $m_{\star,h}$ denote the (positive) effective masses of conduction-band electrons and valence-band holes in the

crystal. These quantities can be calculated analytically from the band structure by expanding the band energies in powers of K up to the second order using $k \cdot p$ perturbation theory (see, e.g., Ref. [34]). While doing so, we apply the two-band approximation again, which means that we neglect contributions to $m_{\star,e}$ and $m_{\star,h}$ from other bands than the valence band and the conduction band. Within this model, we get the well-known relations (cf. Ref. [34])

$$\frac{1}{m_{\star,e}} = \frac{1}{m} + \frac{2\kappa_0^2}{m^2 \mathcal{E}_g},$$
$$\frac{1}{m_{\star,h}} = -\frac{1}{m} + \frac{2\kappa_0^2}{m^2 \mathcal{E}_g} \qquad (33)$$

according to $k \cdot p$ perturbation theory.

By adding these two equations, we find that the effective mass $m_\star$ (27) defined in the previous subsection is given by the harmonic mean of the effective charge-carrier masses:

$$m_\star = \frac{2}{m_{\star,e}^{-1} + m_{\star,h}^{-1}}, \qquad (34)$$

which equals twice the reduced mass. This relation (34) between our effective mass $m_\star$, which is related to κ_0 (off-diagonal momentum matrix element) via Eq. (27), and the parabolic curvatures of the energy bands is essential for extending the analogy at $K = 0$ to a neighborhood of this point with the same effective physical constants $m_\star$ and $c_\star$ as before. Note that we are not required to assume $m_{\star,e} = m_{\star,h}$ here in the time-dependent case in order to draw the analogy.

If we had defined an effective elementary charge $q_\star$ instead of $c_\star$ (as mentioned in the previous subsection), Eq. (34) would not be valid since we would have a different $m_\star$ [given by $\mathcal{E}_g/(2c^2)$] then. For this reason, the analogy would not work for nonzero (quasi)momenta.

Returning to the K derivatives in Eq. (31), we may utilize Eq. (34) to write the energy-band difference in the semiconductor as $\Delta\mathcal{E}(K) = \mathcal{E}_g + K^2/m_\star + \mathcal{O}(K^3)$. As expected at an extremum, we get $\Delta\mathcal{E}^{(1)}(0) = 0$. The group velocity difference Δv is given by the first K derivative of the energy difference, so we get $\Delta v^{(1)}(0) = \Delta\mathcal{E}^{(2)}(0) = 2/m_\star$. The quadratic A term vanishes since $\kappa^{(1)}(0) = 0$ (see Appendix C for the calculation). All in all, we arrive at

$$\Omega(t,K) = \Omega(t,0) + \frac{\mathcal{E}_g q A(t)/(2m_\star)}{\Omega(t,0)} K + \mathcal{O}(K^2)$$
$$\overset{\text{Eq. (28)}}{=} \Omega(t,0) + \frac{c_\star^2 q A(t)}{\Omega(t,0)} K + \mathcal{O}(K^2). \qquad (35)$$

Comparing this result with Eq. (30) confirms the analogy between the Dirac case and the semiconductor case up to the first order in the conserved (quasi)momentum around $k = K = 0$.

E. Analogy in the entire Brillouin zone

The analogy between the Hamiltonians can be extended to the whole Brillouin zone, which means that each K mode in $\hat{H}_s$ can be mapped to a k mode in $\hat{H}_D$ with a suitable effective speed of light and electron mass. In the previous two subsections, we have derived that these effective quantities are constant

(K independent) for long-wavelength modes and that k and K have an interchangeable meaning for these modes. However, this coincidence between k and K is not universal since we can always confine the crystal momentum of a Bloch electron in the two-band semiconductor to the first Brillouin zone (a consequence of restricting ourselves to two bands), while each canonical wave vector in the Dirac case represents a unique mode. The distinction becomes important when we go beyond long-wavelength modes, which we will do in this section.

The question we aim to answer is as follows: Given a semiconductor band structure, i.e., the functions $\Delta\mathcal{E}(K)$, $\Delta v(K) = d\Delta\mathcal{E}(K)/dK$, and $\kappa(K)$ are fixed, and a mode $K \in (-\pi/\ell, \pi/\ell]$, can we then find effective constants $m_\star(K)$ and $c_\star(K)$ and a wave vector $k = k(K)$ such that the eigenvalue $\Omega[t, k(K)]$ in the Dirac case [Eq. (19)] with these K-dependent effective quantities equals the semiconductor analog $\Omega(t, K)$ in Eq. (24)? We therefore want to solve the equation

$$m_\star^2(K)c_\star^4(K) + c_\star^2(K)[k(K) + qA(t)]^2$$
$$= \left[\frac{\Delta\mathcal{E}(K) + qA(t)\Delta v(K)}{2}\right]^2 + \left[\frac{qA(t)|\kappa(K)|}{m}\right]^2 \quad (36)$$

for an arbitrary potential $A(t)$, so we compare the coefficients with respect to the powers of A. This procedure yields three equations, which uniquely fix the three unknown quantities

$$c_\star(K) = \sqrt{\frac{\Delta v^2(K)}{4} + \frac{|\kappa(K)|^2}{m^2}}, \quad (37)$$

$$m_\star(K) = \frac{\Delta\mathcal{E}(K)|\kappa(K)|}{2mc_\star^3(K)}, \quad (38)$$

$$k(K) = \frac{\Delta\mathcal{E}(K)\Delta v(K)}{4c_\star^2(K)}. \quad (39)$$

These K-dependent effective quantities are of course compatible with the results from the previous two subsections: for $K = 0$, we get $c_\star(0) = \kappa_0/m$, $m_\star(0) = \mathcal{E}_g m^2/(2\kappa_0^2)$, and $k(0) = 0$, exactly what we found in Sec. II C. Furthermore, we find that the first K derivatives at $K = 0$ are $c_\star^{(1)}(0) = m_\star^{(1)}(0) = 0$ and $k^{(1)}(0) = 1$; that is, for all long-wavelength modes, the effective quantities are constant, and the crystal momentum K in the semiconductor has the same meaning as the momentum k in Dirac theory, which is basically the result of Sec. II D.

In the remainder of this paper, we will focus on modes with small conserved (quasi)momenta again. For brevity, we write $c_\star$ and $m_\star$ without a parameter again to denote the respective value at $K = 0$. Note that, in the gauge used here, K is conserved exactly for purely time-dependent fields $A(t)$. This is somewhat different from other gauges where K becomes effectively time dependent $K \to K + qA(t)$, and thus the analogy between pair creation and Landau-Zener tunneling during the temporal passage through an avoided level crossing (at the gap $K = 0$) becomes even more apparent. In our representation (where K is conserved), we may directly translate the momentum spectra from QED calculations (e.g., for the dynamically assisted Sauter-Schwinger effect [7,8]) to the semiconductor scenario via Eqs. (37), (38), and (39). The only difference is that the range of K is reduced to the Brillouin zone in the semiconductor case, and the density of states is given per K interval (instead of k for real QED), which introduces an additional factor of dk/dK.

However, when comparing to experimental results, another important difference must be taken into account: the conserved wave numbers K (and k) correspond to the canonical momenta, which are generally different from the mechanical momenta. The latter are not conserved, of course, because the electric field accelerates the charged particles *after* they have been created. This acceleration then depends on the shape of the dispersion relation, such that here the analogy to QED eventually breaks down. Ergo, the analogy applies to the *creation* of particle-hole pairs (for a given K), but not necessarily to their trajectory *after* they have been created.

F. Analog Sauter-Schwinger effect and dynamical assistance in gallium arsenide

The fact that the Hamiltonians $\hat{H}_D$ and $\hat{H}_s$ do coincide for long-wavelength modes (except for scales) allows us to infer that we may directly transfer all findings regarding nonperturbative (tunneling) pair creation from quantum electrodynamics to the semiconductor model (at least to leading order).

1. Constant electric field

Let us start with a constant electric field E_{stat} with $A(t) = E_{stat}t$ as the simplest example. In the Dirac case, this corresponds to the ordinary Sauter-Schwinger effect with the associated critical electric field strength E_{crit}^{QED} [see Eq. (2)]. In a semiconductor, interband tunneling due to a constant external field is typically described via the Landau-Zener model [19–21], but due to the analogy with quantum electrodynamics (QED), we may also use the QED terminology and consequently define the analog critical field strength

$$E_{crit} = \frac{c_\star^3 m_\star^2}{q} = \frac{\sqrt{2m_\star}\mathcal{E}_g^{3/2}}{4q}. \quad (40)$$

This expression, here simply derived from the analogy with QED, can be found in many papers which study the behavior of semiconductors/insulators in strong electric fields; see, e.g., Ref. [35].

As an example for a semiconductor with a direct band gap at the Brillouin-zone center (as assumed in Sec. II C), we consider gallium arsenide (GaAs) here. The band gap of GaAs measures about $\mathcal{E}_g^{GaAs} = 1.5$ eV, and the effective masses $m_{\star,e}^{GaAs} = 0.063m$ and $m_{\star,h}^{GaAs} = 0.076m$ (light holes; see Ref. [36]) yield the value $m_\star^{GaAs} \approx 0.069m$ according to Eq. (34). The resulting critical field strength is thus $E_{crit}^{GaAs} \approx 6.2 \times 10^6$ V/cm, a typical value for this type of semiconductor according to, e.g., Ref. [37]. This value is roughly one order of magnitude larger than the dielectric-breakdown field strength of GaAs given in Ref. [36]. This relation seems reasonable since interband tunneling starts below E_{crit}^{GaAs} of course, but it is suppressed exponentially by the factor $\exp(-\pi E_{crit}^{GaAs}/E_{stat})$. For $E_{stat} \approx E_{crit}^{GaAs}/10$, this factor measures 10^{-14}. We do not consider the (nonexponential) prefactor in the pair-creation rate here, but one can easily imagine that the exponential term suppresses any realistic prefactor for much smaller values of E_{stat}.

2. Assisting temporal Sauter pulse

As a next example, we add a temporal Sauter pulse $E_{\text{Sauter}}/\cosh^2(\omega t)$ to the constant background field E_{stat} and assume that the pulse amplitude is much smaller than the static field: $E_{\text{Sauter}}/E_{\text{stat}} \ll 1$. The effect of the weak pulse on nonperturbative pair creation has been studied in Ref. [6]. According to that paper, the pulse is negligible if its characteristic frequency scale ω is smaller than a certain critical value ω_{crit}, which depends on the background field strength but (interestingly) not on the pulse amplitude. This critical frequency scale is reached when the combined Keldysh parameter

$$\gamma_\omega = \frac{m\omega}{q\,E_{\text{stat}}} = \frac{E_{\text{crit}}^{\text{QED}}}{E_{\text{stat}}}\frac{\omega}{m} \qquad (41)$$

takes on the value $\pi/2$. Above this threshold, the so-called dynamically assisted Sauter-Schwinger effect sets in, which means that the pulse exponentially enhances the pure Sauter-Schwinger pair-creation rate induced by E_{stat}.

Let us assume in our example that the background field is one order of magnitude below the critical field strength. In the Dirac case, that means $E_{\text{stat}} = E_{\text{crit}}^{\text{QED}}/10$, and we get a critical frequency scale in the hard x-ray spectrum: $\omega_{\text{crit}} = 80$ keV. In our semiconductor example ($E_{\text{stat}} = E_{\text{crit}}^{\text{GaAs}}/10$), the result $\omega_{\text{crit}} = 0.12$ eV lies in the infrared part of the spectrum.

3. Assisting harmonic oscillation

The last example profile consists of the constant background field E_{stat} again plus a harmonic oscillation $E_{\text{wave}}\cos(\omega t)$. Similar to the Sauter pulse, such a wave can increase the nonperturbative pair-creation rate exponentially as studied in Ref. [10]. However, the critical value of the Keldysh parameter (41) for dynamical assistance depends on the ratio $E_{\text{wave}}/E_{\text{stat}}$ for this profile or, if ω and E_{stat} are fixed, we can inverse this relation to determine a critical laser amplitude $E_{\text{wave}}^{\text{crit}}$ as a function of E_{stat} and ω.

In the world-line instanton picture, the effect of the additional oscillation is that it lowers the instanton action $\mathcal{A}$, which in turn increases the pair-creation rate since the rate is proportional to $\exp(-\mathcal{A})$. (We ignore the nonexponential prefactor in the pair-creation rate here; however, it has been shown in Ref. [38] that the behavior of the exponent $\mathcal{A}$ plays the crucial role in the dynamical assistance mechanism.) Let us (arbitrarily) define the threshold of dynamical assistance as a configuration according to which the pair-creation rate with the oscillation [$\propto \exp(-\mathcal{A}_\omega)$] is 50% larger than the rate [$\propto \exp(-\mathcal{A}_0)$] in the constant background field E_{stat} alone. We may derive from Eqs. (52) and (57) in Ref. [10] that this condition gives

$$\frac{e^{-\mathcal{A}_\omega}}{e^{-\mathcal{A}_0}} = \exp\left[2\pi\frac{E_{\text{crit}}^{\text{QED}}}{E_{\text{stat}}}\frac{I_1(\gamma_\omega)}{\gamma_\omega}\frac{E_{\text{wave}}}{E_{\text{stat}}}\right] \overset{!}{=} 1.5, \qquad (42)$$

where $I_1(x)$ denotes a modified Bessel function of the first kind. Assuming that only the oscillation amplitude is variable, we solve this equation for E_{wave} to find the critical amplitude

$$E_{\text{wave}}^{\text{crit}} = \frac{\ln 1.5}{2\pi}\frac{E_{\text{stat}}}{E_{\text{crit}}^{\text{QED}}}\frac{\gamma_\omega}{I_1(\gamma_\omega)}E_{\text{stat}}. \qquad (43)$$

TABLE I. Comparison between the scales in the Dirac Hamiltonian and the analog quantities in the semiconductor model.

Dirac theory		Two-band semiconductor
Electron mass m	$\leftrightarrow$	$m_\star$, effective mass [Eqs. (27) and (34)]
		GaAs: $m_\star \approx 0.07m$
Speed of light c	$\leftrightarrow$	$c_\star = \sqrt{\mathcal{E}_g/(2m_\star)}$, effective speed
		GaAs: $c_\star \approx 0.005c$
Mass gap $2mc^2$	$\leftrightarrow$	$2m_\star c_\star^2 = \mathcal{E}_g$, band gap
≈ 1 MeV	$\leftrightarrow$	GaAs: $\mathcal{E}_g \approx 1.5$ eV
Sauter-Schwinger effect:		
$E_{\text{crit}}^{\text{QED}} = m^2c^3/q$	$\leftrightarrow$	$E_{\text{crit}} = \sqrt{2m_\star}\mathcal{E}_g^{3/2}/(4q)$
$\approx 10^{18}$ V/m	$\leftrightarrow$	GaAs: $E_{\text{crit}} \approx 6\times 10^8$ V/m
Dynamically assisted Sauter-Schwinger effect:		
$\omega_{\text{crit}} \approx 80$ keV	$\leftrightarrow$	GaAs: $\omega_{\text{crit}} \approx 0.12$ eV

Let us now transfer this QED result (43) to the semiconductor analog and do some estimations regarding the experimental realization of assisted tunneling pair creation in GaAs. We assume a rather pure sample of GaAs placed in a background field $E_{\text{stat}} = E_{\text{crit}}^{\text{GaAs}}/10$ again. The harmonic oscillation is generated by a CO_2 laser with a wavelength of 10.6 μm. The corresponding photon energy 0.117 eV measures less than 8% of the band gap, so pair creation via multiphoton processes is strongly suppressed. The background field strength and the laser frequency together yield the combined Keldysh parameter $\gamma_\omega = 1.56$. While this value is fixed, we can easily vary the laser amplitude. The critical amplitude (43) is then given by $E_{\text{wave}}^{\text{crit}}/E_{\text{stat}} = 0.0097$ in this example, which corresponds to a laser-beam intensity of $I_{\text{crit}} = (E_{\text{wave}}^{\text{crit}})^2/2 = 47$ kW/cm^2. References [39–41] (which consider only pulsed radiation though) suggest that a GaAs sample of sufficient quality will probably not be destroyed by this amount of incident power; the damage threshold for CO_2-laser pulses with a half-width of 100 ns $= 10^{-7}$ s given in Ref. [41] is of the order of 10 MW/cm^2, for example. We will also show later (in Sec. III D) that the threshold intensity is reduced significantly in a space-dependent static background field of finite spatial extent.

The analog quantities given in this section including the values for GaAs are summarized in Table I.

III. SPACETIME-DEPENDENT CASE $E = E(t,x)$

In this section, we generalize the semiconductor model presented in the previous section to spacetime-dependent electric fields and compare it to the corresponding Dirac Hamiltonian again.

A. Hamiltonians

Here, we choose a different gauge $E(t,x) = \partial_x\Phi(t,x)$, with a vanishing vector potential A; that is, the field is described by the spacetime-dependent scalar potential Φ, which enters the position-space Hamiltonians $\hat{H}_D$ (3) and $\hat{H}_s^{\text{full}}$ (6) as an additional potential term $-q\Phi$. The momentum-space form of the Dirac Hamiltonian thus contains the convolution of the spatial Fourier transform of the scalar potential $\tilde{\Phi}(t,k)$ and the momentum-space field operator $\tilde{\hat{\Psi}}$ [see Eq. (4) for the

conventions we use]:

$$\hat{H}_D(t) = \int_{-\infty}^{\infty} \hat{\underline{\tilde{\Psi}}}^\dagger(t,k) \begin{pmatrix} m & k \\ k & -m \end{pmatrix} \hat{\underline{\tilde{\Psi}}}(t,k) \, dk$$
$$- \frac{q}{\sqrt{2\pi}} \int_{-\infty}^{\infty} \hat{\underline{\tilde{\Psi}}}^\dagger(t,k) \int_{-\infty}^{\infty} \tilde{\Phi}(t,k-k')$$
$$\times \hat{\underline{\tilde{\Psi}}}(t,k') \, dk' \, dk. \tag{44}$$

As in the time-dependent case, we want to bring this Hamiltonian into a form in which the matrix in the upper line is diagonal. This is accomplished by inserting the same transformed field operator $\hat{\underline{\Upsilon}}$ (17) as in the previous section (but with $A = 0$ of course). However, the very same transformation gives rise to a matrix M in the lower ($\tilde{\Phi}$) part of the Hamiltonian. This matrix reads as

$$M(k,k') = \frac{1}{\sqrt{1+d^2(k)}} \frac{1}{\sqrt{1+d^2(k')}}$$
$$\times \begin{pmatrix} 1 & d(k) \\ -d(k) & 1 \end{pmatrix} \cdot \begin{pmatrix} 1 & -d(k') \\ d(k') & 1 \end{pmatrix} \tag{45}$$

with the auxiliary function d defined in Eq. (18) but without any time dependence here ($A = 0$). For the transformed Dirac Hamiltonian, we thus get

$$\hat{H}_D(t) = \int_{-\infty}^{\infty} \hat{\underline{\Upsilon}}^\dagger(t,k) \begin{pmatrix} \Omega(k) & 0 \\ 0 & -\Omega(k) \end{pmatrix} \hat{\underline{\Upsilon}}(t,k) \, dk$$
$$- \frac{q}{\sqrt{2\pi}} \int_{-\infty}^{\infty} \hat{\underline{\Upsilon}}^\dagger(t,k) \int_{-\infty}^{\infty} \tilde{\Phi}(t,k-k') M(k,k')$$
$$\times \hat{\underline{\Upsilon}}(t,k') \, dk' \, dk, \tag{46}$$

again with the same (but time-independent) eigenvalues $\pm\Omega$ from Eq. (19).

Let us now derive the semiconductor Hamiltonian in the spacetime-dependent field. We start with the full Hamiltonian (6) again but with $A = 0$ and the additional potential term $-q\Phi$. After the insertion of the two-band approximation (8), our semiconductor Hamiltonian reads as

$$\hat{H}_s(t) = \int_{-\pi/\ell}^{\pi/\ell} \hat{\underline{a}}^\dagger(t,K) \begin{pmatrix} \mathcal{E}_+(K) & 0 \\ 0 & \mathcal{E}_-(K) \end{pmatrix} \hat{\underline{a}}(t,K) \, dK$$
$$- q \int_{-\pi/\ell}^{\pi/\ell} \hat{\underline{a}}^\dagger(t,K) \int_{-\pi/\ell}^{\pi/\ell} \mathcal{M}(t,K,K')$$
$$\times \hat{\underline{a}}(t,K') \, dK' \, dK \tag{47}$$

with the matrix

$$\mathcal{M}(t,K,K') = \begin{pmatrix} \langle +,K|\Phi|+,K'\rangle & \langle +,K|\Phi|-,K'\rangle \\ \langle -,K|\Phi|+,K'\rangle & \langle -,K|\Phi|-,K'\rangle \end{pmatrix}. \tag{48}$$

Further transformations of the operators $\hat{a}_\pm$ are not necessary in this case since the matrix in the upper line of $\hat{H}_s$ is already diagonal for the present gauge.

It is important to notice here that the diagonal elements $\mathcal{E}_\pm$ in $\hat{H}_s$ are generally not symmetric (for all K) as in the Dirac case ($\pm\Omega$) in Eq. (46). In the purely time-dependent field, we could make these diagonal elements in $\hat{H}_s$ symmetric via a suitable gauge transformation (see Sec. II B). However, the same approach is not valid in a spacetime-dependent field since

the Φ part of the Hamiltonian couples particles with different values of K with each other, so K is not a conserved quantity anymore, and thus $\hat{\underline{a}}^\dagger(t,K)\hat{\underline{a}}(t,K) = 1$ is *not* valid in general here for each K. As we will see in the next subsection, this fact requires us to make an additional assumption concerning the effective masses in the semiconductor in order to draw the quantitative analogy to the Dirac Hamiltonian.

B. Analogy between the Φ-independent parts of the Hamiltonians

At this point, we can start to compare the upper lines of the Hamiltonians $\hat{H}_D$ (46) and $\hat{H}_s$ (47), which do not depend on the potential Φ. We focus on the vicinities of the band gaps at $k = K = 0$ again.

Up to the lowest nonvanishing order of the small quantity k/m near the gap, the diagonal elements in the Dirac case are

$$\pm\Omega(k) = \pm mc^2 \pm \frac{k^2}{2m} + \mathcal{O}\left[\left(\frac{k}{mc}\right)^4\right] \tag{49}$$

with c written explicitly. According to our notion, the analogy to $\hat{H}_s$ is valid if $\pm\Omega$ coincides with $\mathcal{E}_\pm$ [from Eq. (32)] up to the quadratic order in k or K after substituting the physical scales m and c with effective constants. (As in Secs. II C and II D in the case of a purely time-dependent E field, the physical roles of k and K are equivalent close to the gaps.)

We find that the analogy works with the same effective constants $c_\star$ (28) and $m_\star$ (34), as in the $A(t)$ case, but we have to assume in addition that the effective electron mass in the conduction band $m_{\star,e}$ equals the effective hole mass $m_{\star,h}$ (in which case $m_\star = m_{\star,e} = m_{\star,h}$). Graphically, that means that the parabolic curvatures of the energy curves $\mathcal{E}_+$ and $\mathcal{E}_-$ in Fig. 1(b) must be identical at the gap. From a practical point of view, this is an important constraint regarding the simulation of nonperturbative vacuum pair production in spacetime-dependent fields in semiconductors, which can only be met approximately. The effective masses in GaAs, $m_{\star,e}^{\mathrm{GaAs}} = 0.063m$ and $m_{\star,h}^{\mathrm{GaAs}} = 0.076m$ (light holes), differ by about 20%, for example; compared to other common semiconductors with a direct band gap, this is a quite good agreement (values taken from Ref. [36]).

We will assume $m_\star = m_{\star,e} = m_{\star,h}$ in the remainder of this section.

C. Analogy between the Φ parts for spatially slowly varying potentials

We still have to show that the analogy is also true for the Φ parts [lower lines in Eqs. (46) and (47)] of the Hamiltonians in the vicinity of the band gap. We thus have to compare the matrix $\tilde{\Phi}(t,k-k')M(k,k')/\sqrt{2\pi}$ in the Dirac case with $\mathcal{M}(t,K,K')$ in the semiconductor case since the other terms in the Φ parts are equivalent. These matrices cannot be the same for arbitrary (quasi)momenta and potentials $\Phi(t,x)$, so we have to make reasonable assumptions about these quantities and then compare the matrices (approximately).

Let us start with the Dirac case. As we can see in the Hamiltonian (46), the Fourier components of the potential Φ couple particle states which differ by $k - k'$ in their wave vectors. Since we want to concentrate on the parabolic vicinity

of the band gap (the range $|k| \ll m$) and electron transitions therein, we assume that the potential only has nonvanishing Fourier components $\tilde{\Phi}(t,k)$ for small wave vectors which satisfy $|k/m| \ll 1$. That is, the potential and thus the electric field is slowly varying in space compared to the Compton wavelength of an electron, and therefore an electron close to the gap cannot be excited (directly) to a point far beyond the gap in k space.

This assumption is also consistent with the fact that we are interested in nonperturbative pair creation: for this reason, the electric field should only incorporate photon energies far below the mass gap $2m$, which correspond to wave numbers $|k| \ll 2m$, leading basically to the same assumption as above.

For a Dirac-sea electron with a k near the gap ($|k/m| \ll 1$), which may be excited into another state with the small wave vector k' ($|k'/m| \ll 1$) due to the potential, we may therefore Taylor expand the matrix $M(k,k')$ and neglect terms of second order in these small wave vectors. We get

$$M(k,k') = \begin{pmatrix} 1 & 0 \\ 0 & 1 \end{pmatrix} + \frac{k-k'}{2mc} \begin{pmatrix} 0 & 1 \\ -1 & 0 \end{pmatrix}$$
$$+ \mathcal{O}\left[\frac{k^2}{m^2c^2}\right] + \mathcal{O}\left[\frac{(k')^2}{m^2c^2}\right] + \mathcal{O}\left[\frac{kk'}{m^2c^2}\right] \quad (50)$$

with the speed of light written explicitly.

In the semiconductor case, we have to approximate the matrix $\mathcal{M}$ for slowly varying potentials. These are potentials which only include wavelengths much greater than the lattice constant ℓ. We therefore assume that its spatial Fourier transform $\tilde{\Phi}(t,K)$ vanishes except for $|K| \ll 2\pi/\ell$. In analogy to the Dirac case, this K-space region coincides with the parabolic vicinity of the semiconductor band gap; cf. Fig. 1(b).

We think that this long-wavelength assumption is practically always satisfied in the context of nonperturbative electron-hole pair creation, which requires the photon energies in the electric field to be much smaller than the band gap: $\omega \ll \mathcal{E}_g$. Let us do a simple estimate to show this: Writing ω as $2\pi/(n\lambda)$, where n is the refractive index in our semiconductor (for the frequency under consideration), the condition $\omega \ll \mathcal{E}_g$ becomes $\lambda \gg 2\pi/(n\mathcal{E}_g)$. It is generally justified to assume that $\mathcal{E}_g$ is (much) smaller than the Fermi energy $\mathcal{E}_F = \pi^2/(2m\ell^2)$ in the empty lattice. Inserting this relation into the above inequality lets us conclude that $\lambda \gg 2\pi/(n\mathcal{E}_F)$, which can also be written as $\lambda \gg (8/n)(\ell/\lambda_C)\ell$, where $\lambda_C \approx 10^{-12}$ m is the Compton wavelength of the electron. For typical semiconductors, ℓ/λ_C is much greater than 1, while $8/n$ is of order 1. Hence, $\lambda \gg \ell$ should be reasonable to assume provided $\omega \ll \mathcal{E}_g$ for all photons in the external field.

Since we are especially interested in GaAs here, let us consider this case in particular: The assumption $\omega \ll \mathcal{E}_g^{\text{GaAs}} = 1.5$ eV corresponds to vacuum wavelengths much greater than 816 nm. The refractive index of GaAs around the band gap measures about 3.7 (see Ref. [42] and cf., e.g., Ref. [36]), so the wavelengths within the medium must be much greater than approximately 220 nm, a length scale which is very large compared to the lattice constant 0.565 nm of GaAs. The assumption of a slowly varying potential in the semiconductor case is thus not problematic in the context of nonperturbative pair creation in GaAs, and, as argued above, this statement presumably also holds in most other semiconductors.

This assumption together with the fact that we consider quasimomenta obeying $|K| \ll 2\pi/\ell$ and $|K'| \ll 2\pi/\ell$ lets us derive the (still exact) expression

$$\mathcal{M}(t,K,K') = \frac{1}{\sqrt{2\pi}}\tilde{\Phi}(t,K-K')$$
$$\times \begin{pmatrix} \langle +,K|+,K'\rangle_u & \langle +,K|-,K'\rangle_u \\ \langle -,K|+,K'\rangle_u & \langle -,K|-,K'\rangle_u \end{pmatrix}$$
$$(51)$$

for the matrix in Eq. (48); see Appendix D for the calculation.

Since we are close to the band gap, we may expand the Bloch factors which appear in the $\langle \dots \rangle_u$ products [defined in Eq. (11)] around $K = 0$ up to the first order in K or K' using $k \cdot p$ perturbation theory and the two-band approximation again (cf. Appendix C). Inserting these expansions from Eq. (C2) and also using the Bloch-factor orthonormality relation (11) yields

$$\mathcal{M}(t,K,K') = \frac{\tilde{\Phi}(t,K-K')}{\sqrt{2\pi}}\left\{\begin{pmatrix} 1 & 0 \\ 0 & 1 \end{pmatrix} + \frac{\kappa_0(K-K')}{m\mathcal{E}_g}\right.$$
$$\times \begin{pmatrix} 0 & 1 \\ -1 & 0 \end{pmatrix} + \mathcal{O}[K^2]$$
$$\left. + \mathcal{O}[(K')^2] + \mathcal{O}[KK']\right\}. \quad (52)$$

Let us now identify the correct effective scales: We consider the expression $2m_\star c_\star$. According to Eq. (28), this quantity is equal to $\sqrt{2m_\star\mathcal{E}_g}$, which in turn becomes $m\mathcal{E}_g/\kappa_0$ by means of Eq. (27). We can thus write $\mathcal{M}$ as

$$\mathcal{M}(t,K,K') = \frac{\tilde{\Phi}(t,K-K')}{\sqrt{2\pi}}\left\{\begin{pmatrix} 1 & 0 \\ 0 & 1 \end{pmatrix} + \frac{K-K'}{2m_\star c_\star}\right.$$
$$\times \begin{pmatrix} 0 & 1 \\ -1 & 0 \end{pmatrix} + \mathcal{O}[K^2]$$
$$\left. + \mathcal{O}[(K')^2] + \mathcal{O}[KK']\right\}. \quad (53)$$

Comparing this equation to Eq. (50) shows that the Φ parts of the Hamiltonians are equivalent close to the band gaps as well, with the same scale substitutions as before. Hence, we have derived the analogy between $\hat{H}_D$ and $\hat{H}_s$ also in the spacetime-dependent case.

D. Dynamically assisted Sauter-Schwinger effect in the spacetime-dependent case

We close this section by considering an experimentally oriented setup, which is a spacetime-dependent version of the dynamically assisted Sauter-Schwinger effect in a semiconductor analog.

1. Assisting temporal Sauter pulse

A spacetime-dependent QED scenario has been studied analytically in Ref. [11] via the world-line instanton method. In this reference, the superposition of a spatial and a temporal Sauter pulse is considered:

$$E(t,x) = \frac{E_1}{\cosh^2(kx)} + \frac{E_2}{\cosh^2(\omega t)}. \quad (54)$$

(a) Large potential step $q\Delta\Phi \gg \chi$.

(b) Slightly above threshold $q\Delta\Phi = \chi$.

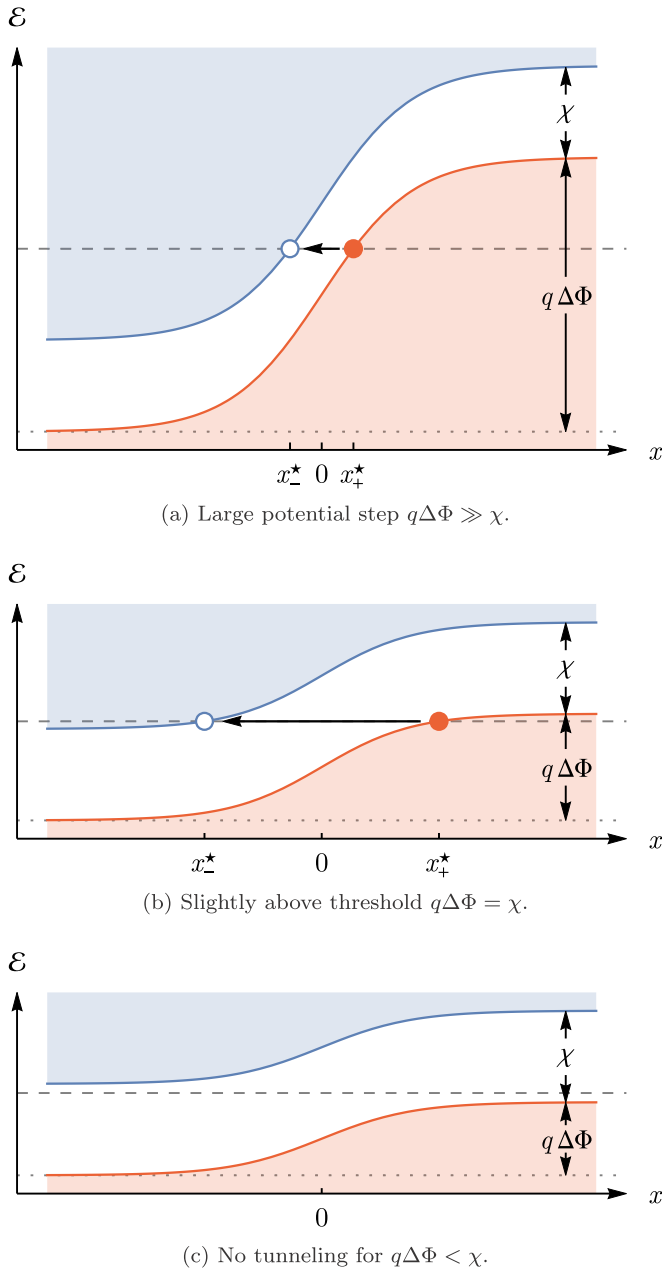(c) No tunneling for $q\Delta\Phi < \chi$.

FIG. 2. Two energy bands separated by a gap χ are bent by a localized, space-dependent electric field centered at $x = 0$ (schematically, tanh profiles). The solid curves are the lower edge of the upper energy band and the upper edge of the lower band, respectively. We have $\chi = 2m$ in QED and $\chi = \mathcal{E}_g$ in the semiconductor analog. (a) For field profiles which give rise to a large potential difference $q\Delta\Phi \gg \chi$, there are many different states between which tunneling is possible (e.g., along the dashed line). (b) For $q\Delta\Phi \searrow \chi$, the number of possible tunneling transitions approaches zero and the spatial turning points $x_\pm^\star$ diverge. In this $\Delta\Phi$ range, the tunneling rate can significantly be increased via additional electric low-frequency pulses according to Ref. [11]. (c) If the energy step $q\Delta\Phi$ is smaller than the gap χ, the bands are separated energetically as indicated by the dashed constant-energy line, so tunneling becomes impossible.

If the spatial pulse is very broad [quasihomogeneous, cf. the linear, middle part in the band diagram in Fig. 2(a)], the "ordinary" dynamically assisted Sauter-Schwinger effect [6]

known from the purely time-dependent case in Sec. II F is recovered. This effect starts at

$$\gamma_\omega^{\mathrm{crit}} = \frac{m\omega_{\mathrm{crit}}}{qE_1} = \frac{\pi}{2}. \tag{55}$$

The spatial turning points (between which tunneling happens) read as $x_\pm^\star = \pm m/(qE_1)$ in this case.

This situation changes when we narrow the spatial pulse $E_1/\cosh^2(kx)$ by increasing its k, while E_1 is kept constant and subcritical here ($E_1 \ll E_{\mathrm{crit}}^{\mathrm{QED}}$). The total electrostatic energy the pulse provides reads as $q\Delta\Phi = 2qE_1/k$. When this energy approaches the mass gap from above, $q\Delta\Phi \searrow 2m$, due to an increasing k, we get a band diagram like in Fig. 2(b). The spatial turning points grow according to $x_\pm^\star \sim \pm|\ln(q\Delta\Phi - 2m)|$ in this limit, so the tunneling rate due to the spatial pulse alone is low then. These turning points are also the positions in Euclidean spacetime where the corresponding instanton trajectory (we are just referring to the spatial Sauter pulse at the moment) crosses the spatial axis (x). The positions $\pm\tau_0$ where this instanton trajectory intersects the τ axis (imaginary time, $\tau = it$) are given by

$$\tau_0 = \frac{m}{qE_1} \frac{\arcsin\gamma_k}{\gamma_k\sqrt{1 - \gamma_k^2}} \tag{56}$$

according to Ref. [43], where

$$\gamma_k = \frac{mk}{qE_1} \tag{57}$$

is the Keldysh parameter of the spatial Sauter pulse. Hence, the positions $\pm\tau_0$ diverge like $1/\sqrt{q\Delta\Phi - 2m}$ in the limit $q\Delta\Phi \searrow 2m$, which is equivalent to $\gamma_k \nearrow 1$; see Ref. [11].

The effect of the additional temporal Sauter pulse $\propto \cosh^{-2}(\omega t)$ is, in the instanton picture, that it gives rise to "walls" at $\pm\tau_{\mathrm{sing}} = \pm\pi/(2\omega)$, which "reflect" the instanton trajectory when touched. The value of ω for which the unperturbed (no temporal pulse) instanton trajectory just touches these "walls" is precisely ω_{crit}, the onset frequency scale for dynamical assistance. The instanton-trajectory scalings explained above let us conclude that $\omega_{\mathrm{crit}} \sim \sqrt{q\Delta\Phi - 2m}$ in the limit $q\Delta\Phi \searrow 2m$; cf. Ref. [11]. Hence, if $q\Delta\Phi$ is only slightly larger than $2m$ [Fig. 2(b)], even low-frequency pulses should lead to an exponential enhancement of nonperturbative (tunneling) pair creation via the dynamically assisted Sauter-Schwinger effect. Since the space dependence of such pulses is slow, their purely time-dependent treatment should be valid.

Now, let us transfer this situation to the semiconductor analog. A localized, time-independent E field within a semiconductor gives rise to the same schematic band diagrams depicted in Fig. 2. For example, the band bending may be due to a suitable doping profile plus an additional external bias if required. The exact form of the bands will not be that of a hyperbolic tangent in general as in Fig. 2, which corresponds to a spatial Sauter-pulse E field $\propto\cosh^2(kx)$. However, we assume that the spatial E field within the semiconductor does also decay exponentially for large $|x|$, just like a spatial Sauter pulse does, but we do not prescribe an exact pulse shape near the field maximum (the region around $x = 0$ in Fig. 2). Note that this assumption is not compatible with the conventional depletion approximation (see, e.g., Ref. [36]) according to

which the density of ionized dopants is piecewise constant, which leads to parabolic potential curves within these ionized regions and constant potential values outside. But, the idea of sharp transitions between ionized and unionized regions is generally considered unrealistic, and one expects "smeared" transitions instead (see Ref. [36]). We think that it is physically reasonable to assume exponential "tails" at the edges of such transitions, which, together with the Boltzmann statistics of the free charge carriers, should lead to a built-in field approaching zero exponentially (far away from $x = 0$). Even if thermal effects are negligible (low temperatures), we nevertheless still expect the built-in field to decay exponentially due to quantum effects: if we think of the ionized, spatially fixed dopants on either side of the junction as creating an effective, finite potential well for the respective majority carriers, the wave functions of these carriers will leak into the forbidden region (which begins somewhere on the other side of the junction), an effect which is in accordance with the exponential decay of the built-in field.

Assuming that the time-independent (built-in) field within the semiconductor decays exponentially, we conclude that the spatial turning points $x_\pm^\star$ scale like $\ln(q\Delta\Phi - \mathcal{E}_g)$ in the critical limit $q\Delta\Phi \searrow \mathcal{E}_g$ [Fig. 2(b)], just like in the QED case above. Now, let us imagine the unperturbed (no additional temporal Sauter pulse) instanton trajectory in this limit: $x_\pm^\star$ will be large, so the instanton trajectory will be a huge closed loop over the x range $[x_-^\star, x_+^\star]$. Except near $x = 0$, where we do not know the exact pulse shape of the spatial field in the semiconductor, the instanton trajectory is the same as that of a spatial Sauter pulse (QED case above) because the E fields in both cases decay exponentially; this functional form is sufficient to fix the shape of the instanton trajectory. The imaginary-time (τ) positions where the instanton trajectory crosses the τ axis will thus also diverge like $1/\sqrt{q\Delta\Phi - \mathcal{E}_g}$ in the limit $q\Delta\Phi \searrow \mathcal{E}_g$. This is because the exponential tails of the field let the instanton trajectory grow so large in this limit that the details close to the maximum field (around $x = 0$) are not important for the scaling anymore. Consequently, we expect the same scaling $\omega_{\mathrm{crit}} \sim \sqrt{q\Delta\Phi - \mathcal{E}_g}$, as in the QED case [11] to be exhibited by an analog of the dynamically assisted Sauter-Schwinger effect in a semiconductor with a localized, time-independent inner field in the limit $q\Delta\Phi \searrow \mathcal{E}_g$ as well.

Note that this scaling law solely depends on the way the electric field approaches zero asymptotically (here, exponentially). See Refs. [44,45] for more information on universal pair-creation phenomena in the no-tunneling limit.

2. Assisting harmonic oscillation

Another way to assist tunneling dynamically in this spacetime-dependent scenario is via a harmonic oscillation instead of a temporal Sauter pulse. This profile,

$$E(t,x) = \frac{E_1}{\cosh^2(kx)} + E_2 \cos(\omega t), \quad (58)$$

is more appropriate to describe experiments in which pair creation is assisted via laser beams, for example. The purely time-dependent version of this profile (homogeneous background field instead of a spatial Sauter pulse) has been studied in Ref. [10], also via the world-line instanton method. In

contrast to the temporal Sauter pulse, the oscillation does not give rise to "walls" (singularities) parallel to the x axis in Euclidean spacetime because $\cos(\omega t) = \cosh(\omega\tau)$ is well behaved for all imaginary times $\tau = it$. Hence, the onset of dynamical assistance by the oscillation is not as sharply defined as in the Sauter-pulse case. We have formulated the threshold condition (43) for the oscillation amplitude E_2 in the case of a homogeneous background field ($k = 0$ limit) in Sec. II F 3 (with $E_{\mathrm{stat}} \to E_1$ and $E_{\mathrm{wave}} \to E_2$ here). Let us now estimate how this critical oscillation amplitude E_2^{crit} changes when the background field becomes a spatial Sauter pulse ($k > 0$), while the maximum background field strength E_1 and the oscillation frequency ω remain fixed.

We consider the instanton trajectory of the spatial Sauter pulse again (see Ref. [43]). This closed loop in Euclidean spacetime has its largest extent [from $-\tau_0$ to $+\tau_0$ with τ_0 from Eq. (56)] in the imaginary-time direction on the τ axis ($x = 0$), where the field strength of the spatial Sauter pulse measures E_1, and that of the oscillation would be $E_2 \cosh(\omega\tau_0)$. We assume that this instanton trajectory will be noticeably deformed (dynamical assistance) by the additional oscillation if the amplitude E_2 is large enough such that the term $E_2 \cosh(\omega\tau_0)$ has a magnitude comparable to E_1. Equation (43) can be understood as defining a certain "threshold ratio" between these two terms for the special case of a homogeneous background field [$k = 0$, in which case $\tau_0 = m/(qE_1)$]:

$$\frac{E_2^{\mathrm{crit}}(k=0)}{E_1} \cosh[\underbrace{\omega\tau_0(k=0)}_{\gamma_\omega}] \overset{!}{=} \mathrm{const}. \quad (59)$$

When we now increase k (i.e., decrease the pulse width), $\tau_0(k)$ grows according to Eq. (56). As a simple estimate, we determine the critical amplitude $E_2^{\mathrm{crit}}(k)$ for this nonzero k by demanding that the constant on the right-hand side of the above equation remains invariant. Hence, $E_2^{\mathrm{crit}}(k > 0)$ must be smaller than $E_2^{\mathrm{crit}}(k = 0)$ to compensate the increase of $\cosh[\omega\tau_0(k > 0)]$. By considering the ratio between both critical amplitudes, we can eliminate the constant and find

$$\frac{E_2^{\mathrm{crit}}(k)}{E_2^{\mathrm{crit}}(k=0)} = \frac{\cosh\gamma_\omega}{\cosh[\omega\tau_0(k)]}. \quad (60)$$

Note that this way to derive $E_2^{\mathrm{crit}}(k)$ is not guaranteed to preserve the property that we have originally imposed to find the critical amplitude in the homogeneous-field case (the oscillation enhances the pair-creation yield by 50%; see Sec. II F 3); rather, we have presented a simple way to estimate how $E_2^{\mathrm{crit}}(k)$ changes when increasing k from zero, and our main intention here is to show that the critical amplitude decreases when the spatial extent of the static background field gets smaller.

By squaring Eq. (60) (and inserting τ_0), we finally find an expression for the critical (laser-beam) intensity as a function of the inverse Sauter-pulse length scale k:

$$\frac{I_{\mathrm{crit}}(k)}{I_{\mathrm{crit}}(k=0)} = \frac{\cosh^2\gamma_\omega}{\cosh^2\left[\gamma_\omega \arcsin(\gamma_k)/\left(\gamma_k\sqrt{1-\gamma_k^2}\right)\right]}, \quad (61)$$

where the threshold for a constant background field $I_{\mathrm{crit}}(k=0)$ can be calculated via Eq. (43). Note that $I_{\mathrm{crit}}(k)$ decreases for
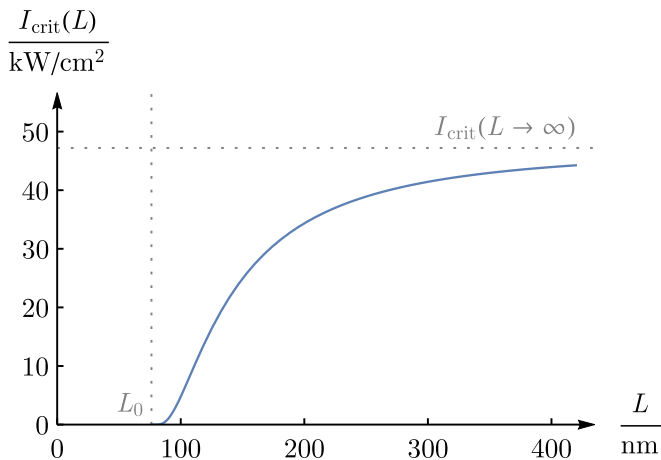
FIG. 3. Threshold CO_2-laser-beam intensity (61) for dynamical assistance of tunneling as a function of the width $L = 2\pi/k$ of the static Sauter pulse $E_1/\cosh^2(kx)$ in GaAs. The parameter values in this plot are $E_1 = E_{\mathrm{crit}}^{\mathrm{GaAs}}/10 \approx 60$ MV/m, $\omega = 0.117$ eV (so $\gamma_\omega = 1.56$), and $I_{\mathrm{crit}}(L \to \infty) = I_{\mathrm{crit}}(k = 0) = 47$ kW/cm^2 (see Sec. II F 3). Tunneling vanishes in the limit $\gamma_k \nearrow 1$ [cf. Fig. 2(b)], which corresponds to $L \searrow L_0 = 76$ nm here.

increasing k until the critical amplitude becomes zero at a certain k value with $\gamma_k = 1$. This is precisely the k value at which tunneling due to the spatial Sauter pulse alone vanishes [cf. Fig. 2(b)], so the concept of assisted tunneling breaks down there. Hence, by decreasing the width of the static background field appropriately, we can make the threshold intensity for dynamical assistance via the oscillation arbitrarily small in principle; however, in order to really verify this effect under controlled conditions in the laboratory, the tunneling currents (assisted and nonassisted) should not become too tiny, so that they remain measurable. This requirement poses a practical limit on how narrow the spatial Sauter pulse (built-in field) may become.

Let us exemplify the result of Eq. (61) for a semiconductor analog by reconsidering the experimental setup from Sec. II F 3 (time-dependent case; i.e., homogeneous fields only): we said there that tunneling pair creation in GaAs induced by a constant background field $E_1 = E_{\mathrm{crit}}^{\mathrm{GaAs}}/10 \approx 60$ MV/m will significantly be assisted by a CO_2-laser wave $E_2 \cos(\omega t)$ (with $\omega = 0.117$ eV fixed, so $\gamma_\omega = 1.56$) if the beam intensity is about $I_{\mathrm{crit}}(k = 0) = 47$ kW/cm^2. If we replace the constant background field with a spatial Sauter pulse $E_1/\cosh^2(kx)$ with an associated length scale $L = 2\pi/k$, Eq. (61) gives us the L-dependent critical laser intensity plotted in Fig. 3.

We emphasize that the dynamical assistance mechanisms from Refs. [6,10,11] considered here are fully nonperturbative effects, which are based on a classical-field description of the external fields. So, even though we assume the assisting temporal Sauter pulse and the time-dependent oscillation to be weak in amplitude ($E_2 \ll E_1 \ll E_{\mathrm{crit}}^{\mathrm{QED}}$), they still must incorporate a large number of photons (high intensity) as to allow for the classical field picture. The dynamically assisted Sauter-Schwinger effect in semiconductors should thus not be confused with the Franz-Keldysh effect [46,47] (see also Refs. [48]), which is related to a shift in the photon-absorption

edge. The QED analog of this effect was considered in Refs. [49–51].

IV. GENERALIZATION TO ELECTROMAGNETIC FIELDS IN 2+1 DIMENSIONS

In this section, we briefly discuss the feasibility to generalize the analogy between Bloch electrons and holes in semiconductors and Dirac's theory to 2+1 spacetime dimensions, including known results.

The step from one to two spatial dimensions is interesting because it also allows for external magnetic fields, not just electric fields as in the one-dimensional case. The Dirac field operator $\hat{\underline{\Psi}}$ still has two components in two dimensions since there is a third Pauli matrix (σ_x) for the additional required gamma matrix γ^2. This absence of spin simplifies the calculations and is typically irrelevant in the context of tunneling pair creation [43,48]. In two-dimensional space, the magnetic field is scalar and acts like the B_z component for charge carriers confined to the (x, y) plane in three dimensions. It is given by the components of the vector potential $\vec{A}(t, x, y)$ via $B = -\partial_x A_y + \partial_y A_x$.

Graphene (see Refs. [52,53]) is a well-known example for a two-dimensional system which mimics relativistic electron motion near the points where the conduction band touches the valence band in the Brillouin zone (Dirac cones); see also Ref. [31]. However, the associated effective electron rest mass is zero, so the analog of the Schwinger limit $E_{\mathrm{crit}}^{\mathrm{QED}} \propto m^2$ vanishes in graphene, and thus there is no characteristic exponential suppression of the Sauter-Schwinger effect; see Refs. [15,16]. But, by generating an offset (symmetry breaking) between the two triangular carbon lattices, which in combination make up the honeycomb structure of graphene, it is possible to separate both energy bands by a finite-energy gap. The Dirac cones of this so-called semiconducting graphene become shaped like paraboloids near the gaps, which corresponds to a nonvanishing effective rest mass. Semiconducting graphene has already been produced successfully in the laboratory via epitaxial growth as reported in Ref. [54], and it has been studied in Ref. [17] as an analog for electron-positron pair creation in constant and oscillating (in time) electric fields.

One possible problem with analogs of Dirac's theory in multiple space dimensions is that the vacuum is isotropic, so m and c are scalar quantities, while material properties of semiconductors, for example, can depend on direction (effective mass tensor, direction-dependent effective speed of light, etc.). Since these anisotropies have no counterpart in Dirac theory, we focus on materials which behave isotropically around the band gap (scalar effective quantities) or at least whose anisotropies do not interfere for the electromagnetic field profile under consideration.

A simple profile which is interesting to study in 2+1 dimensions consists of perpendicular electric (x direction) and magnetic fields, both constant. In Dirac theory, the magnetic field decreases the pair-creation rate induced by the E field because we can always Lorentz-transform to a frame according to which the magnetic field is zero and the pair-creating electric field measures $E^2 - B^2$; see, e.g., Refs. [4,55]. That means that Sauter-Schwinger pair creation vanishes completely for strong enough magnetic fields ($B = E/c$ or higher in SI units). In

Ref. [29], the authors state that for the same reason the equivalent effect also happens in a two-band semiconductor, but again with the effective scales $m \to m_\star$ and $c \to c_\star$ [Eqs. (28) and (34)]. (As in Sec. III B, we have to assume $m_{\star,e} = m_{\star,h} = m_\star$ here.) Their reasoning is that the electrons in the semiconductor obey an effective Dirac equation (near the band gap) since this type of equation models a simple two-band system. The validity of a Dirac-type equation implies the existence of an analog Lorentz transformation (with $c \to c_\star$), which is then used to show that tunneling vanishes for $B = E/c_\star$ in the semiconductor. More detailed explanations of this Dirac-type two-band model are given in Refs. [28,48], which also study the crossed-field profile, and in Refs. [30,31].

We can understand the reduction of Landau-Zener tunneling in a semiconductor due to a perpendicular B field as well by starting with the same approach as in the previous sections, which deal with the QED-semiconductor analogy in 1+1 dimensions. That is, we begin with the Schrödinger Hamiltonian (6) again but for 2+1 dimensions and with the vector potential $\vec{A}(x) = -Bx\vec{e}_y$ and the additional scalar potential $\Phi(x) = Ex$ (crossed constant fields). We then insert the (2+1)-dimensional version of the two-band approximation (8). The resulting two-band Hamiltonian contains first- and second-order derivatives with respect to the component K_x of the crystal momentum, which arise from the Bloch-basis representations of x and x^2 (see, e.g., Refs. [32,56,57] for the calculation of these matrix elements). As a simple, semiclassical approach, we then consider just the center of the Brillouin zone $\vec{K} = 0$ (where we, again, assume the direct band gap to be located) and derive the corresponding x-dependent band energies from the Hamiltonian ($i\partial_{K_x} \to x$). What we find is an expression which looks similar to the relativistic counterpart

$$\mathcal{E}_\pm(x) = -qEx \pm \sqrt{m^2c^4 + (cqBx)^2} \qquad (62)$$

(for the same crossed-field profile and $\vec{k} = 0$) but with the known effective constants $c \to c_\star$ and $m \to m_\star$, plus additional terms under the square root. However, these additional terms can be neglected for typical values $m_\star/m \approx 10^{-2}\text{–}10^{-1}$, $c_\star/c \approx 10^{-3}\text{–}10^{-2}$ (see the data for GaAs in Table I, for example), a not too strong tunneling-inducing electric field $E \approx 10^{-1} E_{\text{crit}} \approx 10^7$ V/m, a perpendicular magnetic field in the range $B \lesssim E/c_\star \approx 10$ T, and x values of the order of the unperturbed (by the B field) tunneling length $\mathcal{E}_g/(qE)$. The $\mathcal{E}_\pm(x)$ graphs in the semiconductor thus look like the relativistic version, which was also found in Ref. [48].

We emphasize that the reduction of the tunneling current in perpendicular B fields has just been explained by referring to the local dispersion relations of the Dirac equation and the two-band semiconductor model, respectively. So, although the same effect happens in both systems, this does not necessarily imply the analogy between the full underlying Hamiltonians/equations of motion.

V. CONCLUSIONS

We studied the quantitative analogy between the Sauter-Schwinger effect and interband tunneling in suitable semiconductors with special emphasis on fields which depend on space and time. To this end, we compared the Dirac Hamiltonian [Eqs. (5) and (44)] in 1+1 dimensions with the effective two-band Hamiltonian of a semiconductor [Eqs. (15) and (47)]. In the case of purely time-dependent electric fields $E(t)$, one may derive a quantitative analogy for every k mode after a spatial Fourier transform. In this case, the analog of the Schwinger critical field (40) is determined by material constants such as the band gap $\mathcal{E}_g$ and the interband coupling κ_0, which is related to the effective mass $m_\star$ via Eq. (27). For GaAs, for example, we obtain a value of approximately $E_{\text{crit}}^{\text{GaAs}} \approx 6.2 \times 10^8$ V/m, which is far below the QED critical field $E_{\text{crit}}^{\text{QED}} \approx 1.3 \times 10^{18}$ V/m and about one order of magnitude above the typical breakdown field strength of a few (3–9) 10^7 V/m in GaAs according to Ref. [36]. This is a very natural result because the analog of the QED critical field yields the ultimate quantum limit until which the semiconductor can retain its insulating behavior: no matter how perfect and free of defects the sample is and how low the temperature, tunneling will become strong at that field strength (unless it is suppressed, e.g., by a magnetic field; see below).

This scenario of purely time-dependent electric fields $E(t)$ would already allow us to study the analog of the dynamically assisted Sauter-Schwinger effect [6] with an additional Sauter pulse, for example, where the threshold frequency (for $E_{\text{stat}} = E_{\text{crit}}^{\text{GaAs}}/10$) lies around 0.12 eV (instead of 80 keV as in real QED), which is favorable for an experimental verification. For the experimentally probably more relevant case of an additional sinusoidal field (instead of a Sauter pulse), we get the additional requirement that the field strength of this additional field should be large enough to assist tunneling. This indicates an important difference to the well-known Franz-Keldysh effect [46,47] corresponding to tunneling assisted by a single photon (which can be treated perturbatively). A single photon with an energy of 0.12 eV would not have a significant impact because its energy is far below the band gap. However, a field oscillating at this frequency with sufficient intensity can assist tunneling, which shows that it is necessary to treat this field beyond (first-order) perturbation theory; see also Refs. [10,58].

For electric fields depending on space and time, $E(t,x)$, more approximations are necessary to obtain a quantitative analogy. For example, because electrons and positrons in real QED are limited by the same speed of light, one has to neglect the difference in the velocities of particles and holes (more precisely, the curvature of their bands at the gap) in the semiconductor and to approximate both by the same effective mass of around 7% of the electron mass. This scenario $E(t,x)$ includes additional interesting cases. For example, if the strong and static field is inhomogeneous and close to the edge of the tunneling regime, the frequency and/or field strength of the additional weaker time-dependent field required for dynamical assistance is reduced; see Sec. III D and Ref. [11].

Finally, we discussed the generalization to 2+1 dimensions. Apart from facilitating the distinction between transverse and longitudinal fields (see also Ref. [10]), this case also allows us to introduce a magnetic field. For the Sauter-Schwinger effect in real QED, it is well known that an additional magnetic field can suppress the tunneling probability. Here, we find an analogous suppression for the tunneling in semiconductors; see also Refs. [28,29,48]. For example, in GaAs with an electric field of 1% of the critical field, $E_{\text{stat}} = E_{\text{crit}}^{\text{GaAs}}/100$ (i.e., roughly one order of magnitude below the breakdown field strength),

a magnetic field of 1 Tesla can already suppress tunneling significantly ($E_{stat}/c_\star^{GaAs} \approx 4.5$ T will stop it completely).

In summary, our findings suggest that the analog of the Sauter-Schwinger effect and its dependence on the spatial and temporal field profile (e.g., dynamical assistance) should be observable with present-day technology in suitable high-quality semiconductors at low temperatures, where competing mechanisms (due to defects, etc.) are suppressed sufficiently.

VI. OUTLOOK: INTERACTIONS

In all of our previous considerations, we neglected the Coulomb interaction between the electrons. This approximation is well motivated experimentally since the picture of noninteracting electrons (e.g., band structure, Drude model) describes the experiments in bulk semiconductors typically very well. Note that the situation is different in quantum dots, for example, where the spatial confinement enhances Coulomb interaction effects.

The same approximation is typically used in real QED, where most of the calculations regarding the Sauter-Schwinger effect neglect the interaction between the created electrons and positrons. While this interaction is expected to be small, it is probably fair to say that it is not fully understood yet.

In order to obtain a rough estimate, let us compare the Coulomb force $F_{Coulomb}$ of the electron-positron pair separated by the tunneling distance to the force $F_{ext} = qE$ induced by the external electric field:

$$\frac{F_{Coulomb}}{F_{ext}} = \frac{1}{4}\alpha_{QED}\frac{E}{E_{crit}^{QED}}. \tag{63}$$

Thus, even for a very strong field of $E = E_{crit}^{QED}/10$, we find a suppression of $\approx 2 \times 10^{-4}$, which indicates that neglecting these interactions is a good approximation.

If we now perform the same estimate for the semiconductor case, we find

$$\frac{F_{Coulomb}}{F_{ext}} = \frac{1}{4}\alpha_{QED}\frac{E}{E_{crit}}\frac{c}{c_\star}. \tag{64}$$

As a result, due to $c/c_\star \approx 217$ for GaAs (cf. Table I), the impact of the Coulomb interactions is stronger in this situation. Intuitively speaking, the electrons are slower and thus have more time to interact. This enhancement is even more pronounced for graphene [52] where $c/c_\star \approx 300$. Nevertheless, even with the very strong field $E = E_{crit}^{GaAs}/10$, the Coulomb force is only a 4% correction to the external force, such that neglecting it should still be a good approximation.

Turning the argument around, high-precision experiments in semiconductors could (at least qualitatively) illuminate the impact of interactions, while the analogous experiments in real QED are far more difficult.

APPENDIX A: ABSORPTION OF THE A^2 TERM IN THE SEMICONDUCTOR HAMILTONIAN

In the time-dependent case (Sec. II), the electric potential is specified in temporal gauge, that is, $E(t) = \dot{A}(t)$ and the scalar potential Φ is set to zero. However, introducing also the scalar potential Φ explicitly for the moment, the electric field becomes $E = \dot{A} + \partial_x\Phi$, so a purely time-dependent scalar potential $\Phi = \Phi(t)$ does not have any physical significance. The scalar potential couples to time derivatives ($\partial_t \to \partial_t - iq\Phi$) and therefore leads to the additional term $-q\Phi$ in the Hamiltonian (6):

$$\hat{H}_s^{full}(t) = \int_{-\infty}^{\infty}\hat{\psi}^\dagger\left\{\frac{[-i\partial_x + qA(t)]^2}{2m} + V(x) - q\Phi\right\}\hat{\psi}\,dx. \tag{A1}$$

We may thus absorb the quadratic A term in this equation by setting $\Phi(t) = qA^2(t)/(2m)$ and obtain the simplified Hamiltonian (7).

APPENDIX B: BLOCH-WAVE MOMENTUM MATRIX ELEMENTS

1. Underlying formula

Let us first derive a general equation for a type of integral which appears regularly in calculations in the Bloch-wave basis. Assume that $g(x)$ is an ℓ-periodic function, i.e., $g(x + \ell) = g(x)$, and we want to calculate the integral $\int_{-\infty}^{\infty}\exp(ikx)g(x)\,dx$ with a real k satisfying $|k| < 2\pi/\ell$.

We start by writing the ℓ-periodic g as a Fourier series

$$g(x) = \sum_{j=-\infty}^{\infty}\tilde{g}_j e^{2\pi ijx/\ell}, \tag{B1}$$

with complex Fourier coefficients $\tilde{g}_j$. Insertion into the above integral yields

$$\int_{-\infty}^{\infty}e^{ikx}g(x)\,dx = \sum_{j=-\infty}^{\infty}\tilde{g}_j\int_{-\infty}^{\infty}e^{i(k+2\pi j/\ell)x}\,dx$$
$$= 2\pi\sum_{j=-\infty}^{\infty}\tilde{g}_j\,\delta\left(k + \frac{2\pi}{\ell}j\right). \tag{B2}$$

Since $|k| < 2\pi/\ell$, the delta distribution vanishes except for the case $j = 0$; cf., e.g., Ref. [59]. The corresponding Fourier coefficient $\tilde{g}_0$ coincides with the average of g over a unit cell, so we get the result

$$\int_{-\infty}^{\infty}e^{ikx}g(x)\,dx = \frac{2\pi}{\ell}\int_0^\ell g(x)\,dx\,\delta(k). \tag{B3}$$

2. Momentum matrix elements

We start to calculate the matrix elements by inserting the general Bloch wave form (10):

$$\langle n,K| - i\partial_x|n',K'\rangle$$
$$= \int_{-\infty}^{\infty}f_n^*(K,x)(-i\partial_x)f_{n'}(K',x)\,dx$$

$$= \int_{-\infty}^{\infty} e^{i(K'-K)x} u_n^*(K,x)$$

$$\times \left[K' u_{n'}(K',x) - i \frac{\partial u_{n'}(K',x)}{\partial x} \right] dx. \quad \text{(B4)}$$

Since the Bloch factors are ℓ periodic with respect to x and $|K' - K| < 2\pi/\ell$ (because K and K' are restricted to the first Brillouin zone), we may apply Eq. (B3) and find

$$\langle n,K| - i\partial_x |n',K'\rangle$$
$$= [K \underbrace{\langle n,K|n',K\rangle_u}_{\delta_{nn'}} + \langle n,K| - i\partial_x |n',K\rangle_u] \delta(K'-K) \quad \text{(B5)}$$

(cf., e.g., Ref. [32]). Note that we used the unit-cell scalar product defined in Eq. (11) to write the remaining single-cell integrals. Furthermore, the first product just gives a Kronecker delta due to the Bloch-factor orthonormalization (11).

APPENDIX C: TAYLOR EXPANSION OF $\kappa(K)$ AROUND $K = 0$

We are interested in the first-order K dependence of κ [Eq. (13)], so we need to evaluate the first K derivative of κ at $K = 0$. Together with the definition of the single-cell product in Eq. (11), we get (K derivatives are denoted as superscript numbers in parentheses)

$$\kappa^{(1)}(0) = \langle u_-^{(1)}(0,x) | -i\partial_x | u_+(0,x)\rangle_u$$
$$+ \langle u_-(0,x) | -i\partial_x | u_+^{(1)}(0,x)\rangle_u. \quad \text{(C1)}$$

The K derivatives of the Bloch factors at $K = 0$ can be calculated by expanding $u_\pm(K,x)$ in powers of K via $k \cdot p$ perturbation theory. Again, we apply the two-band approximation, so we only take into account corrections from the valence band and the conduction band. The resulting expansions

$$u_\pm(K,x) = u_\pm(0,x) \pm \frac{\kappa_0 K}{m\mathcal{E}_g} u_\mp(0,x) + \mathcal{O}(K^2) \quad \text{(C2)}$$

(cf. Ref. [34]) inserted above immediately give

$$\kappa^{(1)}(0) = \left\langle -\frac{\kappa_0}{m\mathcal{E}_g} u_+(0,x) \left| -i\partial_x \right| u_+(0,x) \right\rangle_u$$
$$+ \left\langle u_-(0,x) \left| -i\partial_x \right| \frac{\kappa_0}{m\mathcal{E}_g} u_-(0,x) \right\rangle_u$$
$$= -\frac{\kappa_0}{\mathcal{E}_g} \Delta v(0) = 0 \quad \text{(C3)}$$

since the group velocities $v_\pm(K) = \langle \pm, K| - i\partial_x | \pm, K\rangle_u / m$ vanish at the direct band gap at $K = 0$ in both energy bands.

The Taylor series of κ around $K = 0$ thus does not include a linear term (according to $k \cdot p$ perturbation theory and the two-band model): $\kappa(K) = \kappa_0 + \mathcal{O}(K^2)$.

APPENDIX D: MATRIX ELEMENTS OF $\mathcal{M}(t,K,K')$ FOR SPATIALLY SLOWLY VARYING POTENTIALS

The elements of the matrix $\mathcal{M}(t,K,K')$ in Eq. (48) are expressions of the form $\langle n,K|\Phi|n',K'\rangle$. For slowly varying potentials, this general scalar product can be calculated. We start by inserting the Bloch-wave form (10) and the spatial Fourier transform [cf. Eq. (4)] of the potential. After changing the order of integration, we get

$$\langle n,K|\Phi|n',K'\rangle = \frac{1}{\sqrt{2\pi}} \int_{-\infty}^{\infty} \tilde{\Phi}(t,k)$$
$$\times \int_{-\infty}^{\infty} e^{i(k+K'-K)x} u_n^*(K,x)$$
$$\times u_{n'}(K',x) \, dx \, dk. \quad \text{(D1)}$$

Let us now reconsider our assumptions: The slowly varying potential satisfies $\tilde{\Phi}(t,k) = 0$ unless $|k| \ll 2\pi/\ell$, so we only need to calculate the x integral (correctly) for small values of k. Furthermore, we are interested in the quasimomentum region near the band gap to draw the analogy to Dirac theory; that is, we evaluate the matrix elements between values of K and K' near the Brillouin-zone center and thus $|K' - K|$ is significantly smaller than $2\pi/\ell$, the total zone width. Altogether, we may assume $|k + K' - K| < 2\pi/\ell$ and thus apply the formula in Eq. (B3) again:

$$\langle n,K|\Phi|n',K'\rangle = \frac{1}{\sqrt{2\pi}} \int_{-\infty}^{\infty} \tilde{\Phi}(t,k) \delta(k+K'-K)$$
$$\times \frac{2\pi}{\ell} \int_0^\ell u_n^*(K,x) u_{n'}(K',x) \, dx \, dk. \quad \text{(D2)}$$

Now, the k integral can easily be calculated and the single-cell x integral is expressed via the Bloch-factor scalar product introduced in Eq. (11). That yields our end result

$$\langle n,K|\Phi|n',K'\rangle = \frac{\tilde{\Phi}(t,K-K')}{\sqrt{2\pi}} \langle n,K|n',K'\rangle_u. \quad \text{(D3)}$$

Note that this equation is exact as long as the condition mentioned above is true.

[1] F. Sauter, Über das Verhalten eines Elektrons im homogenen elektrischen Feld nach der relativistischen Theorie Diracs, Z. Phys. **69**, 742 (1931).

[2] F. Sauter, Zum 'Kleinschen Paradoxon', Z. Phys. **73**, 547 (1932).

[3] W. Heisenberg and H. Euler, Folgerungen aus der Diracschen Theorie des Positrons, Z. Phys. **98**, 714 (1936).

[4] J. Schwinger, On gauge invariance and vacuum polarization, Phys. Rev. **82**, 664 (1951).

[5] V. S. Popov, Pair production in a variable and homogeneous electric field as an oscillator problem, Zh. Eksp. Teor. Fiz. **62**, 1248 (1972) [Sov. Phys.–JETP **35**, 659 (1972)].

[6] R. Schützhold, H. Gies, and G. Dunne, Dynamically Assisted Schwinger Mechanism, Phys. Rev. Lett. **101**, 130404 (2008).

[7] M. Orthaber, F. Hebenstreit, and R. Alkofer, Momentum spectra for dynamically assisted Schwinger pair production, Phys. Lett. B **698**, 80 (2011).

[8] C. Fey and R. Schützhold, Momentum dependence in the dynamically assisted Sauter-Schwinger effect, Phys. Rev. D **85**, 025004 (2012).

[9] C. Kohlfürst, M. Mitter, G. von Winckel, F. Hebenstreit, and R. Alkofer, Optimizing the pulse shape for Schwinger pair production, Phys. Rev. D **88**, 045028 (2013).

[10] M. F. Linder, C. Schneider, J. Sicking, N. Szpak, and R. Schützhold, Pulse shape dependence in the dynamically assisted Sauter-Schwinger effect, Phys. Rev. D **92**, 085009 (2015).

[11] C. Schneider and R. Schützhold, Dynamically assisted Sauter-Schwinger effect in inhomogeneous electric fields, J. High Energy Phys. 02 (2016) 164.

[12] N. Szpak and R. Schützhold, Quantum simulator for the Schwinger effect with atoms in bichromatic optical lattices, Phys. Rev. A **84**, 050101 (2011).

[13] N. Szpak and R. Schützhold, Optical lattice quantum simulator for quantum electrodynamics in strong external fields: Spontaneous pair creation and the Sauter–Schwinger effect, New J. Phys. **14**, 35001 (2012).

[14] V. Kasper, F. Hebenstreit, M. K. Oberthaler, and J. Berges, Schwinger pair production with ultracold atoms, Phys. Lett. B **760**, 742 (2016).

[15] D. Allor, T. D. Cohen, and D. A. McGady, Schwinger mechanism and graphene, Phys. Rev. D **78**, 096009 (2008).

[16] B. Dóra and R. Moessner, Nonlinear electric transport in graphene: Quantum quench dynamics and the Schwinger mechanism, Phys. Rev. B **81**, 165431 (2010).

[17] I. Akal, R. Egger, C. Müller, and S. Villalba-Chávez, Low-dimensional approach to pair production in an oscillating electric field: Application to band gap graphene layers, Phys. Rev. D **93**, 116006 (2016).

[18] E. A. Martinez, C. A. Muschik, P. Schindler, D. Nigg, A. Erhard, M. Heyl, P. Hauke, M. Dalmonte, T. Monz, P. Zoller, and R. Blatt, Real-time dynamics of lattice gauge theories with a few-qubit quantum computer, Nature (London) **534**, 516 (2016).

[19] L. D. Landau, Zur Theorie der Energieübertragung. II, Phys. Z. Sowjet. **2**, 46 (1932).

[20] C. Zener, Non-adiabatic crossing of energy levels, Proc. R. Soc. (London) A **137**, 696 (1932).

[21] C. Zener, A Theory of the Electrical Breakdown of Solid Dielectrics, Proc. R. Soc. (London) A **145**, 523 (1934).

[22] L. Hrivnák, Relativistic analogies in direct-gap semiconductors, Prog. Quantum Electron. **17**, 235 (1993).

[23] J. Rau and B. Müller, From reversible quantum microdynamics to irreversible quantum transport, Phys. Rep. **272**, 1 (1996).

[24] W. Zawadzki, Zitterbewegung and its effects on electrons in semiconductors, Phys. Rev. B **72**, 085217 (2005).

[25] T. Oka and H. Aoki, Ground-State Decay Rate for the Zener Breakdown in Band and Mott Insulators, Phys. Rev. Lett. **95**, 137601 (2005).

[26] S. A. Smolyansky, A. V. Tarakanov, and M. Bonitz, Vacuum particle creation: Analogy with the bloch theory in solid state physics, Contrib. Plasma Phys. **49**, 575 (2009).

[27] E. O. Kane, Band structure of indium antimonide, J. Phys. Chem. Solids **1**, 249 (1957).

[28] W. Zawadzki and B. Lax, Two-Band Model for Bloch Electrons in Crossed Electric and Magnetic Fields, Phys. Rev. Lett. **16**, 1001 (1966).

[29] A. G. Aronov and G. E. Pikus, Tunnel current in a transverse magnetic field, J. Exptl. Theoret. Phys. (U.S.S.R.) **51**, 281 (1966) [Sov. Phys.–JETP **24**, 188 (1967)].

[30] W. Zawadzki and T. M. Rusin, Zitterbewegung (trembling motion) of electrons in semiconductors: A review, J. Phys.: Condens. Matter **23**, 143201 (2011).

[31] W. Zawadzki, Electron dynamics in crystalline semiconductors, Acta Phys. Pol. A **123**, 132 (2013).

[32] B. Gu, N. H. Kwong, and R. Binder, Relation between the interband dipole and momentum matrix elements in semiconductors, Phys. Rev. B **87**, 125301 (2013).

[33] N. W. Ashcroft and N. D. Mermin, *Solid State Physics* (Brooks/Cole, Cengage Learning, Belmont, CA, 2008).

[34] P. Y. Yu and M. Cardona, *Fundamentals of Semiconductors*, 4th ed. (Springer, Berlin, 2010).

[35] E. O. Kane, Zener tunneling in semiconductors, J. Phys. Chem. Solids **12**, 181 (1959).

[36] S. M. Sze and K. Ng Kwok, *Physics of Semiconductor Devices*, 3rd ed. (Wiley, New York, 2006).

[37] J. B. Krieger and G. J. Iafrate, Time evolution of Bloch electrons in a homogeneous electric field, Phys. Rev. B **33**, 5494 (1986).

[38] C. Schneider and R. Schützhold, Prefactor in the dynamically assisted Sauter-Schwinger effect, Phys. Rev. D **94**, 085015 (2016).

[39] J. L. Smith, Surface damage of GaAs from 0.694- and 1.06-μ laser radiation, J. Appl. Phys. **43**, 3399 (1972).

[40] J. L. Smith, Effects of Laser Flux on GaAs, in *Laser Induced Damage In Optical Materials: 1973*, edited by A. J. Glass and A. H. Guenther (National Bureau of Standards, Boulder, CO, 1973), pp. 103–106.

[41] J. L. Smith and G. A. Tanton, Intense laser flux effects on GaAs, Appl. Phys. **4**, 313 (1974).

[42] M. N. Polyanskiy, Refractive index database, http://refractiveindex.info

[43] G. V. Dunne and C. Schubert, Worldline instantons and pair production in inhomogenous fields, Phys. Rev. D **72**, 105004 (2005).

[44] H. Gies and G. Torgrimsson, Critical Schwinger Pair Production, Phys. Rev. Lett. **116**, 090406 (2016).

[45] H. Gies and G. Torgrimsson, Critical Schwinger pair production. II. Universality in the deeply critical regime, Phys. Rev. D **95**, 016001 (2017).

[46] W. Franz, Einfluß eines elektrischen Feldes auf eine optische Absorptionskante, Z. Naturforsch. A **13**, 484 (1958).

[47] L. V. Keldysh, The effect of a strong electric field on the optical properties of insulating crystals, J. Exptl. Theoret. Phys. (U.S.S.R.) **34**, 1138 (1958) [Sov. Phys.–JETP **7**, 788 (1958)].

[48] M. H. Weiler, W. Zawadzki, and B. Lax, Theory of tunneling, including photon-assisted tunneling, in semiconductors in crossed and parallel electric and magnetic fields, Phys. Rev. **163**, 733 (1967).

[49] G. V. Dunne, H. Gies, and R. Schützhold, Catalysis of Schwinger vacuum pair production, Phys. Rev. D **80**, 111301 (2009).

[50] A. Monin and M. B. Voloshin, Photon-stimulated production of electron-positron pairs in an electric field, Phys. Rev. D **81**, 025001 (2010).

[51] A. Monin and M. B. Voloshin, Semiclassical calculation of photon-stimulated Schwinger pair creation, Phys. Rev. D **81**, 085014 (2010).

[52] K. S. Novoselov, A. K. Geim, S. V. Morozov, D. Jiang, M. I. Katsnelson, I. V. Grigorieva, S. V. Dubonos, and A. A. Firsov, Two-dimensional gas of massless Dirac fermions in graphene, Nature (London) **438**, 197 (2005).

[53] A. H. Castro Neto, F. Guinea, N. M. R. Peres, K. S. Novoselov, and A. K. Geim, The electronic properties of graphene, Rev. Mod. Phys. **81**, 109 (2009).

[54] M. S. Nevius, M. Conrad, F. Wang, A. Celis, M. N. Nair, A. Taleb-Ibrahimi, A. Tejeda, and E. H. Conrad, Semiconducting Graphene from Highly Ordered Substrate Interactions, Phys. Rev. Lett. **115**, 136802 (2015).

[55] L. D. Landau and E. M. Lifshitz, *The Classical Theory of Fields*, 3rd ed. (Pergamon, Oxford, 1971).

[56] E. N. Adams, Motion of an electron in a perturbed periodic potential, Phys. Rev. **85**, 41 (1952).

[57] E. N. Adams, The Crystal Momentum as a Quantum Mechanical Operator, J. Chem. Phys. **21**, 2013 (1953).

[58] G. Torgrimsson, C. Schneider, J. Oertel, and R. Schützhold, Dynamically assisted Sauter-Schwinger effect: Non-perturbative versus perturbative aspects, J. High Energy Phys. 06 (2017) 043.

[59] J. M. Luttinger and W. Kohn, Motion of electrons and holes in perturbed periodic fields, Phys. Rev. **97**, 869 (1955).